

Enforcing conservation of axial angular momentum in
the atmospheric general circulation model CAM6

Thomas Toniazzo^{1,2}
Mats Bentsen¹
Cheryl Craig³
Brian Eaton³
James Edwards³
Steven Goldhaber³
Christiane Jablonowski⁴
Peter H. Lauritzen³

¹NORCE Klima and Bjerknes Centre for Climate Research, Bergen, Norway

²Department of Meteorology (MISU), Stockholm University, Stockholm, Sweden

³National Center for Atmospheric Research, Boulder, Colorado, USA

⁴University of Michigan, Ann Arbor, Michigan, USA

January 16, 2020

1 Corresponding author's address:
2 Thomas Toniazzo
3 NORCE Research AS
4 Bjerknes Centre for Climate Research
5 Geophysical Institute, Jahnebakken 5
6 Bergen, Hordaland, Norway NO-5070
7 e-mail: thomas.toniazzo@uni.no

Numerical general circulation models of the atmosphere are generally required to conserve mass and energy for their application to climate studies. Here we draw attention to another conserved global integral, viz. the component of angular momentum (AM) along the Earth’s axis of rotation, which tends to receive less consideration. We demonstrate the importance of global AM conservation in climate simulations on the example of the Community Atmosphere Model (CAM) with the finite-volume (FV) dynamical core, which produces a noticeable numerical sink of AM. We use a combination of mathematical analysis and numerical diagnostics to pinpoint the main source of AM non-conservation in CAM-FV. We then present a method to enforce global conservation of AM, and we discuss the results in a hierarchy of numerical simulations of the atmosphere of increasing complexity. In line with theoretical expectations, we show that even a crude, non-local enforcement of AM conservation in the simulations consistently results in the mitigation of certain persistent model biases.

1 Introduction

The atmosphere exchanges angular momentum (AM) with the material bodies at the surface which are, to a good approximation, in a state of motion consisting in uniform rotation about the planetary axis connecting the poles. Per unit of mass, surface AM increases in quadratic proportion to its distance from the planetary axis of rotation, from zero at the poles to a maximum at the Equator. AM is a constant of motion of the dynamical (e.g. Newton’s) equations, so that as air travels meridionally, it carries a specific AM that increasingly differs from that of the Earth’s surface. A variety of mechanisms redistribute atmospheric AM and eventually lead to an exchange of AM between the atmosphere and the surface, mainly as a result of low-level wind shear (“surface stress”) and of small-scale wave motions over steep surface topography (“form drag”).

In the general circulation of the atmosphere, air warms and rises in the zone of semi-permanent convective activity at low latitudes, and travels towards higher latitudes. As it does so, it carries a specific AM that increasingly differs from that at the surface, until AM is exchanged with the surface by a variety of mechanisms. The most important of such mechanisms are turbulent stresses generated by low-level wind shear (“surface stress”) and pressure torques over surface topography (“form drag”). Atmospheric AM is thus lost, mostly in the mid-latitude surface westerlies. The surface branch of this circulation, whereby air travels back towards the equator, requires the opposite exchange of AM between the atmosphere and the surface.

The importance for the atmospheric circulation of conservation of AM in the free troposphere and of AM exchange of air with the surface was recognised long ago. Already in 1735, George

43 Hadley, Esq, F.R.S., noted that without the Assistance of the diurnal Motion [i.e. rotation] of
44 the Earth, Navigation [...] would be very tedious (Hadley 1735), due to the absence of the trade
45 winds. This insight still lies at the core of modern conceptual models for the atmospheric circu-
46 lation (Schneider, 1977; Held and Hou, 1980; Lindzen and Hou, 1988; Pauluis, 2004; Walker and
47 Schneider, 2006). In the upper branch of the Hadley Circulation (HC), the advection of plane-
48 tary angular momentum determines a sharp acceleration of the zonal wind in the mid-latitudes,
49 linked with a front-like drop in air temperatures, marking the location of the subtropical jets
50 (STJs). Partly by baroclinic instability, the mid-latitude circulation redistributes atmospheric
51 AM vertically and produces intense surface westerlies, where the air loses AM to the surface.
52 The equatorward return flow in the surface branch of the HC in turn results in easterly “trade”
53 winds, where surface stresses replenish atmospheric AM until air is lifted in cumulus convection
54 within the inter-tropical convergence zone (ITCZ).

55 This circulation is the object of numerical simulations with general circulation models (GCMs)
56 used in meteorological forecasting and in climate modelling. They describe the atmosphere as
57 a thin, density-stratified, rotating gaseous spherical shell. These properties allow the introduc-
58 tion of a convenient set of approximations in the equations of motion, which result in a system
59 known as the Hydrostatic Primitive Equations (HPEs). The reader is referred to White et al.
60 (2005) for a detailed analysis and discussion. Given suitable boundary conditions, the HPEs
61 guarantee the global conservation of three fundamental physical quantities: mass; energy; and
62 AM along the Earth’s rotation axis. Analytic expressions of these laws can be found e.g. in
63 Laprise and Girard (1990). The three conservation laws determine the fundamental character of
64 the large-scale circulation of the atmosphere, and virtually every climate application of GCMs is
65 sensitive to their enforcement when the continuum equations are discretized in space and time.
66 For example, the effects of changes in radiative forcing of 2 W/m^2 (e.g. IPCC AR5, Chapter
67 8, pg 697) can only be simulated if the model’s energy conservation is significantly better than
68 1%. Estimates based on ECMWF reanalysis data suggest that conservation of AM of a simi-
69 lar precision is desirable for an accurate representation of the annual cycle and of interannual
70 variations of the atmospheric circulation in model simulations (e.g. Egger and Hoinka 2005).

71 CAM, the Community Atmosphere Model developed and maintained at the National Center
72 for Atmospheric Research (NCAR) in Boulder, Colorado, is one of the Atmospheric General
73 Circulations Models (AGCM) in most widespread use today. It also constitutes the core at-
74 mospheric component of NorESM, the Norwegian Earth System Model. Although it offers a
75 choice of dynamical cores, the finite-volume (FV) dynamical core (Lin 2004) has been, and in

76 many instances still is, the default option. The FV dynamical core is exactly mass and vorticity
77 conserving, and it has been employed in all model integrations submitted by NCAR and by the
78 Norwegian Climate Centre (NCC) for the 5th phase of the Coupled Model Inter-comparison
79 Project (CMIP) contributing to the Assessment Report (AR) of the Intergovernmental Panel
80 for Climate Change (IPCC 2013); it is also expected to be used for phase 6 of CMIP by both
81 institutions. Due to its high numerical efficiency, FV also continues to be the code of choice for
82 all uses where overall availability of supercomputing resources is a limiting factor. This includes
83 long historical or palaeoclimate simulations; studies with coupled chemistry and/or carbon cy-
84 cle; seasonal-to-decadal coupled forecasts; academic research; and all model development efforts
85 currently underway with NorESM.

86 In this paper, we employ CAM with the FV dynamical core at two standard CESM resolution
87 only, a coarser one of $1.9^\circ \times 2.5^\circ$ in latitude and longitude, respectively (“f19” for short), and
88 a finer one of $0.9^\circ \times 1.25^\circ$ (“f09”). In agreement with previous results (Lauritzen et al., 2014;
89 Lebonnois et al., 2012), we find that all existing simulations with CAM FV, from CMIP5 to
90 present development versions of CAM6, have a numerical sink of global AM of a magnitude of
91 about 30% of physical sources at f19 resolution, and about 15% at f09 resolution.

92 Figure 1 shows the spurious AM source in aquaplanet (AP; Neale and Hoskins, 2000; Black-
93 burn et al., 2013) and Held-Suarez (HS; Held and Suarez 1994) simulations with CAM FV, and
94 an otherwise identical simulation, but with using the global spectral dynamical core with T42
95 truncation. Although many other models also do not conserve AM, CAM FV is peculiar in
96 producing a sink nearly everywhere, resulting in a particularly large global non-conservation.

97 First principles (e.g. Held and Hou, 1980; Einstein, 1926) suggest that dissipation of AM,
98 equivalent to a body force acting on the fluid as a sink of zonal momentum, forces a secondary
99 circulation with the same sign as the Hadley circulation. As a result, the simulated Hadley
100 circulation may become too vigorous. Reduced meridional advection of zonal momentum may
101 lead to mid-latitude Westerlies that are too weak or displaced poleward. The zonal momentum
102 lost to the non-physical sink must be balanced by a matching additional eastward torque, for
103 example in an expanded or excessively intense area of tropical easterly surface winds. Model
104 simulations with CAM FV consistently tend to reflect such phenomenology: for example, Feldl
105 and Bordoni (2016) and Lipat et al. (2017) show that among CMIP5 models, those based
106 on the FV dynamical core (GFDL-x, CCSM4 and NorESM-x) simulate both relatively large
107 overturning mass flux in the HC, and a high latitude of its edge.

108 It is useful to illustrate these effects of AM non-conservation by means of idealised AGCM ex-

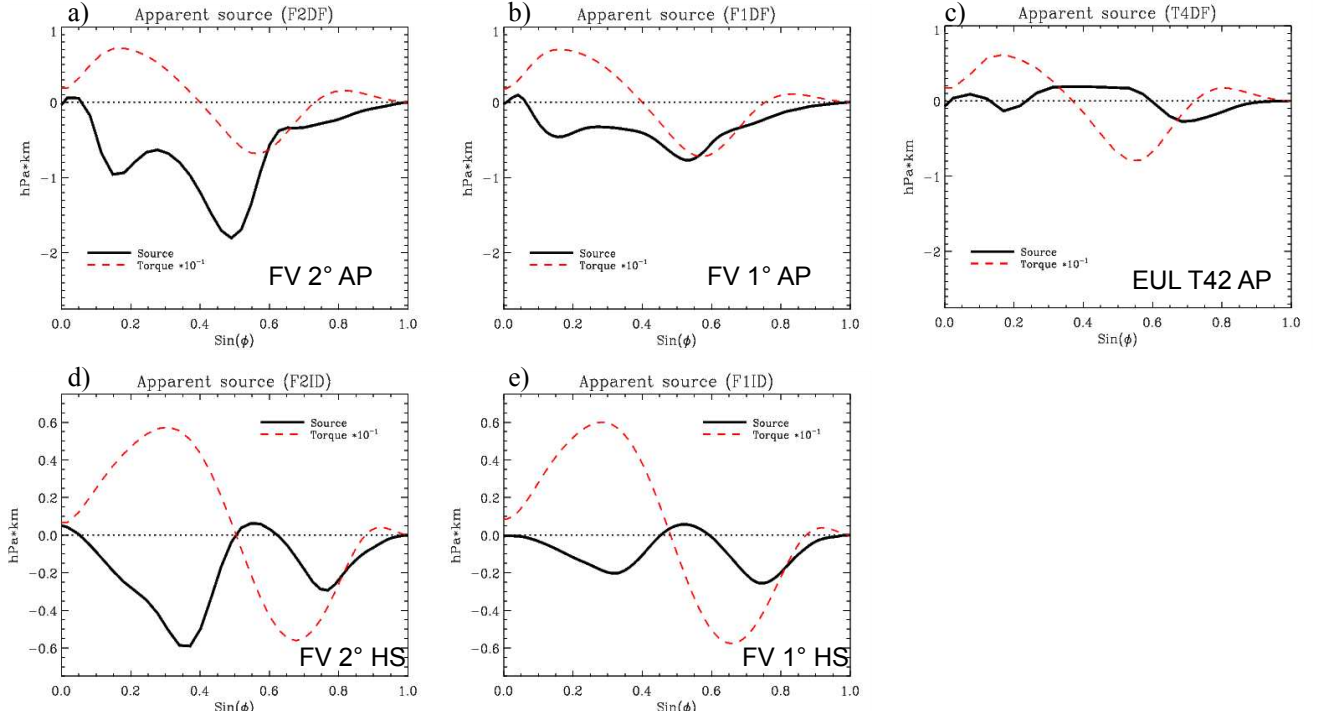


Figure 1: Numerical torque in idealised CAM simulations. The vertically and zonally integrated apparent numerical torque is shown as a function of latitude for CAM simulations in Aquaplanet (AP; panels a), b) and c) in the top row) and Held-Suarez (HS; panels d) and e) at the bottom) configurations. The numerical torque here is obtained as a time-average residual of the tendency of angular momentum in each cylindrical shell of constant latitude of the model’s domain, after subtracting the contributions from meridional convergence and from the surface stress torque. The details of the calculation are in Appendix A. Two simulations with the FV dynamical core are shown for each configuration, one at f19 resolution (i.e. on a regular latitude-longitude grid with spacing of $1.9^\circ \times 2.5^\circ$; panels a) and d)), and one at f09 (i.e. with twice that resolution; panels b) and e)). For comparison, also a CAM simulation in AP configuration with the global spectral dynamical core at quadratic triangular truncation T42 (roughly comparable to FV at f19 resolution) is shown in panel c). The dashed red line in each panel indicate the physical torque from surface stresses, scaled by a factor 0.1. Positive values indicate an eastward torque acting on the atmosphere, and negative values indicate a westward torque acting on the atmosphere.

109 periments that do not include complicating factors such as orographic form drag or parametrised
 110 bulk stresses associated with gravity waves. Figure 2 shows the surface torques resulting from
 111 four solutions for the mean circulation with CAM in AP mode. One of these is obtained directly
 112 from integrations of CAM using the FV dynamical core at f19 resolution (black line). An oth-
 113 erwise identical integration with the global spectral-transform dynamical core at T42 spectral
 114 truncation (green line) is chosen for comparison as a bone-fide example of an AM conserving
 115 simulation (cf Figure 1).

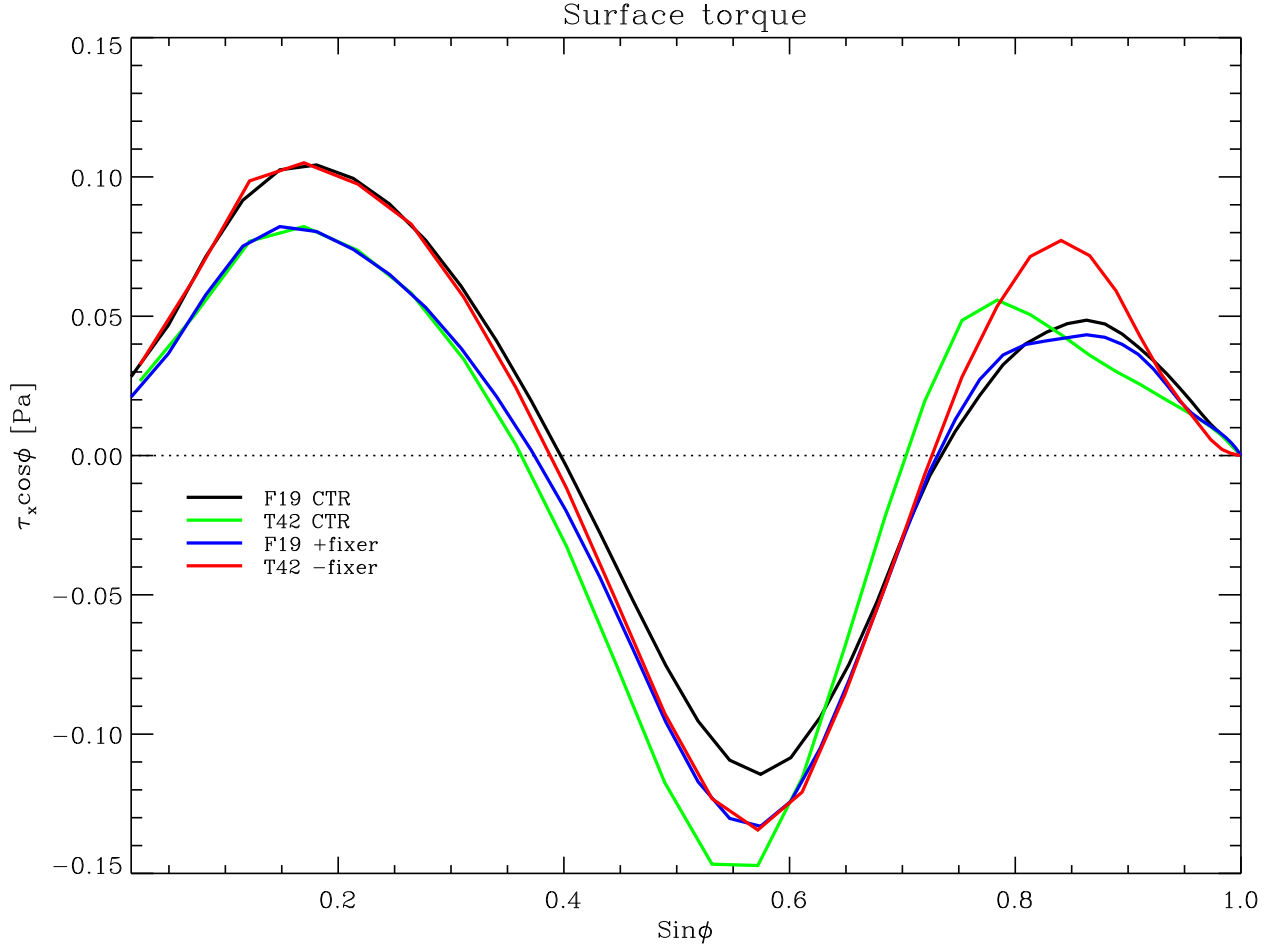


Figure 2: Impact of AM sink in CAM-FV integrations. Meridional distribution of the surface stress torque (analogous to the dashed red lines in Figure 1) in CAM simulations in AP configuration. Two integrations with the FV dynamical core (black and blue lines), and two simulations with the global spectral dynamical core (green and red lines) are shown. One of each pair of integrations is a control case (black and green lines), the other (blue and red lines) is an experiment where an additional solid-body angular acceleration is applied to the entire atmosphere at each time-step of the integration. The acceleration is diagnosed as the time mean of the ratio between the global total numerical torque in the FV control integration and the moment of inertia of the atmosphere. That acceleration is then applied with a negative sign in the FV experiment (blue curve), with the effect of compensating for the numerical torque and achieving approximate global AM conservation in that integration. For the experiment with the spectral dynamical core (red curve), the acceleration is applied with unchanged sign, causing a sink of AM approximately equal to that of the control FV integration. The numerical sink of the control spectral integration is nearly vanishing.

116 The other two integrations, represented by the blue and red lines, are perturbed in identical,
 117 but opposite manner. First, the global-total numerical torque due to the FV dynamical core was

118 diagnosed at every time-step of the reference FV simulation, and averaged in time afterwards.
119 This was converted into a solid-body axial rotation tendency that was applied continuously
120 everywhere as a constant sink of AM in a new integration with the spectral dynamical core,
121 resulting in the simulation represented by the red curve. Vice-versa, the opposite additional
122 solid-body rotation tendency was applied to a new FV integration, thus compensating its internal
123 numerical sink. This integration produced the physical torque represented by the blue curve.
124 Comparing the different curves, it may be seen that Equatorward of about 23 degrees of latitude
125 the simulated physical torque depends primarily on the global budget of atmospheric AM. In
126 particular, notwithstanding the complications of interactive moist physics and the different
127 spatial and temporal discretisations used in the two integrations, the stronger trade winds
128 (in terms of surface stress) in the FV simulation compared with the T42 simulation can be
129 explained entirely with the non-physical, numerical torque of the FV dynamical core. The
130 result is insensitive to how that torque is in fact applied. Even at subtropical and middle
131 latitudes, half of the difference between the two simulations, in terms of surface stresses, can be
132 explained in this way. Similar results are found for the zonal-mean meridional circulation and
133 for the surface pressure in the HC (Figure S1 in the Supplementary Information), confirming
134 the strength and robustness of the Einstein (1926) “tea-leaves” mechanism.

135 These results motivate us to address the issue of AM conservation in the CAM’s FV dynamical
136 core. One may speculate that systematic biases in surface stresses due to the numerical sink
137 of AM must also impact coupled ocean-atmosphere climate simulations, with excessive Ekman
138 and Sverdrup forcing of the subtropical gyres. The northward displacement of the mid-latitude
139 westerlies may also result in excessive mechanical and thermal forcing of the subpolar gyres with
140 possible implications for the Atlantic meridional overturning circulation.

141 In this paper, we propose ways to address numerical dissipation of AM in CAM-FV sim-
142 ulations. Section 2 describes our main hypotheses as to the root cause of the error, and our
143 approaches towards rectification. Section 3 presents the result of our corrections in a set of
144 idealised simulations. The impact on realistic simulations of the atmospheric circulation is
145 discussed in Section 4. Conclusions are finally offered in Section 5.

2 Analysis of potential causes and approaches to correction.

The FV dynamical core (Lin 2004) solves the HPE by updating first the advective (C-grid) and then the prognostic (D-grid) winds in two steps. The first step represents pure advection, i.e. the increments associated with transport, including geometric and Coriolis terms. In this step, the scheme conserves absolute vorticity exactly for the D-grid winds (Lin and Rood 1997; hereafter LR97). The second step calculates the wind increments associated with hydrostatic pressure forces. These are computed in a special way (Lin 1997) that differs from most Arakawa and Lamb (1980) type schemes. Violations of AM conservation may occur in either sub-step.

2.1 Pressure-gradient force

We first analysed the Lin's (1997) treatment of the pressure-gradient terms for conservation. A general discussion is given by Simmons and Burridge (1980), who introduce a set of hybrid-level dimensionless variables, a_k , defined as $a_k := (\phi_k - \phi_{k+1/2})/2(\alpha p)_k$ (in Simmons and Burridge these variables are denoted by α_k ; we change the notation here to avoid confusion), where ϕ is the geopotential, p the pressure, $\alpha := -\partial_\eta \phi / \partial_\eta p$ the specific volume, and η is the generalised or hybrid vertical coordinate. Here and in the following, the index k refers to the vertical level, or to half-levels as appropriate, and subscripts to the partial derivative symbol indicate differentiation with respect to the variable in subscript, $\partial_X \equiv \partial / \partial X$. The variables a_k need not be constants. Simmons and Burridge (1980) derive the discrete form that pressure and geopotential terms must take in general vertical coordinates in order to ensure conservation of axial angular momentum. Their Equation (3.8) can be generalised to:

$$(\alpha \partial_\lambda p + \partial_\lambda \phi)_k = - \left(\frac{\Delta \phi}{\Delta p} \right)_k \partial_\lambda p_{k-1/2} + \partial_\lambda \phi_{k+1/2} + \frac{1}{\Delta p_k} \partial_\lambda [a_k (\alpha p)_k \Delta p_k] , \quad (1)$$

where the symbol Δ is employed to represent a difference between vertical levels, $\Delta p_k := p_{k+1/2} - p_{k-1/2}$ (and similarly for ϕ), and λ is the longitude.

Performing Lin's (1997) path integration around the finite-volume element on this expression yields the following form for the body force:

$$\oint \phi dp = \delta_\lambda \{ [\phi_{k+1/2} + a_k (\alpha p)_k] \Delta p_k \} - \Delta (\overline{\phi \delta_\lambda p})_k \quad (2)$$

where δ_λ is the finite-difference operator in the zonal direction, and $\overline{\phi_{k\pm 1/2}}$ is an average over λ .

172 An expression identical in form to Lin’s (1997) Equation (11) is then recovered if the choices

$$a_k = \frac{\Delta\phi_k}{2(\alpha p)_k}, \quad \bar{\phi} = \frac{\phi_{i+1/2} + \phi_{i-1/2}}{2}, \quad (3)$$

173 are made, where i is the index corresponding to the longitude λ .

174 In other words, Lin’s (1997) expression for the pressure-gradient term is consistent with
175 Simmons and Burridge (1980) prescription for AM conservation, provided that the physical
176 pressure variable p is used in the integration in place of the general pressure function indicated
177 by the symbol π in Lin (1997). This can be directly verified algebraically by summing all
178 expressions of the form of the numerator in the right-hand side of Equation (11) in Lin (1997)
179 along all longitudes and levels. Provided ϕ is constant at one model boundary, and p at the
180 other, it always returns zero. This is the required result provided that the denominator on the
181 right-hand side of Eq.(11) in Lin (1997) represent the inertial mass associated with the velocity
182 points. They do so if π is the hydrostatic pressure.

183 Accordingly, we performed tests in which the integration variable in the relevant section of
184 CAM-FV’s dynamical core was replaced with true interface pressure. The effect was generally
185 seen to be very small on the dynamical core’s momentum conservation properties.

186 We note however that in the CAM implementation there may be an additional problem, asso-
187 ciated with the use of the D-grid. The application of Lin’s (1997) method would strictly require
188 a C-grid, with zonal velocity points interleaving pressure (scalar) points along the same latitude.
189 Thus, in CAM pressure is interpolated to the grid-cell corners before use. While the formal ex-
190 pressions for the pressure forces do not change, thus ensuring S&B’s total torque constraints,
191 the inertial mass associated with each D-grid U -point is in fact averaged over six scalar point
192 surrounding it, with 1-2-1 weights along the zonal direction. This additional zonal smoothing
193 effectively adds spurious terms to the zonal momentum equation, of the form $-u\partial_x^2\Delta p$. This is
194 a potential source of non-conservation. However, it is not expected to be systematic.

195 **2.2 Geometry, polar filtering, and FFSL extension**

196 AM conservation may be affected by the treatment of geometric terms in latitude-longitude
197 coordinates, especially near the poles where such terms become large. Furthermore, convergence
198 of the meridians forces filtering of the solution, and additional approximations to be made. In
199 particular, LR97 implement a flux-form semi-Lagrangian extension of Colella and Woodward’s
200 (1984) PPM algorithm which is used near the poles where CFL numbers become large during

201 the time integration. We performed several sensitivity tests on each of these aspects, without
202 being able to notice significant impacts on AM conservation.

203 Particularly compelling is the comparison with the performance of a prototype implementa-
204 tion in CAM of the FV3 scheme on a cubed-sphere grid (“FV3”), which lacks any poles and does
205 not require or use any of these special formulation (and is, in particular, run in pure Eulerian
206 mode, i.e. without the flux-form semi-Lagrangian extension described in Lin and Rood, 1996).
207 We ran an AP simulation on the C48 grid, viz. six pseudo-cubic faces with 48x48 grid-cells each,
208 for total number of grid-points identical to the standard 2-degree FV configuration, but a 25%
209 higher resolution at the Equator. The AM sink (Figure S2 in the Supplementary Information)
210 is nevertheless comparable, i.e. about 25% smaller, consistently with the scaling with the res-
211 olution of simulations with standard FV. We conclude that FV and FV3 suffer from the same
212 problem, independent of geometry or the FFSL extension of LR97.

213 In order to minimise the impact of other minor (and partly intentional) numerical sources
214 and sinks of AM, in all idealised numerical tests presented in this paper we applied the following
215 modifications: 1. the order of the advection scheme is kept the same (4th) for all model layers,
216 instead of reducing it to 1st in the top layer and to 2nd up to the 8-th layer; 2. an additional
217 conservation check is applied in the vertical remapping of zonal wind and column momentum
218 is conserved in the moist-mass adjustment at the end of physics; 3. the surface-stress residual
219 resulting from closure of the diffusion operator (in physics) is applied in full rather than partially.

220 **2.3 Discretisation of the kinetic-energy term**

221 The evidence from our theoretical and diagnostic analysis points at the advective, shallow-water
222 part of the implementation of LR97 in CAM-FV as the root of the AM conservation error. Its
223 ”vector-invariant” formulation (Arakawa and Lamb 1981) allows for different forms of the diver-
224 gence to be used in the momentum and in the mass and tracer equations, resulting in inconsistent
225 values for the divergence of the flux of planetary AM (associated with mass divergence) and of
226 the flux of relative AM (associated with momentum divergence). In the momentum equations,
227 the divergence is contained in a kinetic-energy (KE) gradient term, which due to the presence of
228 a numerical symmetric instability (Hollingworth et al., 1983) is expressed as the local gradient
229 of a Lagrangian-average KE. Its form violates the finite-volume approximations used for other
230 quantities, e.g. vorticity. This feature is intrinsic to the LR97 numerical discretisation scheme
231 and cannot be eliminated.

232 To address the resulting violation of AM conservation, we first note that even in AM-

233 conserving schemes, conservation can only be guaranteed in the zonal average (Simmons and
 234 Burridge, 1980). We therefore do not attempt a local correction to the scheme, which is li-
 235 able to numerical instabilities (Hollingworth et al., 1983), and instead formulate a zonal-mean
 236 correction as follows. We enforce the AM conservation law:

$$\int d\lambda \partial_t (\Delta p u a \cos^2 \varphi) = - \int d\lambda \partial_\varphi (\Delta p u v \cos^2 \varphi) + \int d\lambda \Delta p f v a \cos^2 \varphi \quad (4)$$

237 by adding a zonal-mean zonal-wind tendency term to the "vector-invariant" form:

$$\begin{aligned} \partial_{t,c} \bar{u} &= \frac{1}{\int d\lambda \Delta p} \\ &\times \left\{ \int d\lambda \Delta p \left(\frac{1}{a \cos \varphi} \partial_\lambda K - \zeta v \right) - \int d\lambda \frac{1}{a \cos^2 \varphi} \partial_\varphi (\Delta p u v \cos^2 \varphi) - \int d\lambda u \partial_t \Delta p \right\}. \end{aligned} \quad (5)$$

238 Here, K is the KE plus the contribution from explicit divergence damping used in FV. In the
 239 continuum limit the expression on the right-hand side reduces simply to the mass-weighted zonal
 240 average of the zonal gradient of $K - (u^2 + v^2)/2$.

241 In discrete form, the last two terms must be approximated. In the C-D grid formulation of
 242 the LR97 scheme the second one is especially problematic. Various possibilities were explored,
 243 which resulted in various degrees of accuracy and stability. The best compromise is to discretise
 244 it as

$$\frac{1}{a \cos^2 \varphi} \partial_\varphi (\Delta p u v \cos^2 \varphi) = \frac{1}{a \cos^2 \varphi} [\Delta p v \partial_\varphi (u \cos \varphi) + u \partial_\varphi (v \Delta p \cos \varphi)], \quad (6)$$

245 allowing some confusion between prognostic D-grid winds and time-centred advective (C-grid)
 246 winds. The details of the derivation are given in Appendix B. Using the mass conservation
 247 equation, this approximation allows us to discretize the two last terms together and write the
 248 zonal-wind correction increment in a form consistent with LR97:

$$\delta_c \bar{u} = \frac{1}{\int d\lambda \overline{\Delta p}_{t+\delta t}} \left\{ \int d\lambda \overline{\Delta p} \left[\frac{\delta t}{a \cos \varphi \delta \lambda} \delta_\lambda K - \overline{\mathcal{Y}(v^*, \delta t; \zeta_\lambda)} \right] + \bar{u}^t \mathcal{F}(u^*, \delta t; \overline{\Delta p}) + O(\delta t^2) \right\}. \quad (7)$$

249 Here, $\zeta_\lambda := \frac{1}{a \cos \varphi} \partial_\lambda v$, and the notation of LR97 is used for the discrete transport operators \mathcal{Y}
 250 and \mathcal{F} , for the meridional transport of ζ_λ and the zonal transport of mass, respectively. The first
 251 three terms in the integrand of Eq.(7) thus correspond to the first three terms on the right-and
 252 side of Eq.(A11) in Appendix B. The last symbol on the right-hand side of Eq.(7) represents
 253 higher-order terms (also detailed in Eq.(A11)). We will refer to this modification of the LR97
 254 scheme as the "correction".

2.4 Diagnostic tools and global conservation

Irrespective of whether the correction, as described above, is applied or not, for diagnostic purposes we calculate the apparent non-physical torque associated with the FV dynamical core advective tendencies only, i.e. excluding the increments associated with pressure gradients. These tendencies are diagnosed separately for each layer at every advective sub-step, and integrated horizontally to yield the apparent numerical global-total torque during the sub-step. At the same time, the layer effective moment of inertia over the sub-step is also computed.

The opposite of the ratio of these quantities gives an angular acceleration that, applied to the zonal wind in each layer at every advective sub-step, enforces conservation of AM of that layer under advection. The application of this solid-body rotation increment at each dynamical time-step and for each layer independently is what we call the “level” fixer. The details of the computation are given in Appendix C.

Irrespective of whether they are actually applied, the fixer’s velocity increments, Eq.(A13), are vertically interpolated and accumulated over the entire dynamic time-step, and written out diagnostically. In addition to the fixer, partial wind and pressure tendencies arising from the dynamical core are separately diagnosed and written to the standard output streams, providing additional diagnostic tools for cross-checking.

A variant of the fixer was tested in CAM simulations. This variant is a “global” fixer, which still acts by applying an increment to the zonal wind at each time-step. In this fixer, the apparent torque and the moment of inertia are integrated over all levels within the domain over which strict overall angular momentum conservation is desired. The zonal wind increments are then applied as a single solid-body rotational acceleration within this domain. Experimentation showed that such acceleration should not be applied in the stratosphere, where conservation errors are small and the impact of unphysical zonal accelerations large. The necessary limitation of the domain for the global fixer however introduces a certain degree of arbitrariness in its application. Although sometimes used for diagnostic purposes, we do not discuss this global fixer variant any further.

Lin’s (2004) FV scheme conserves mass and absolute vorticity exactly. The AM modifications, described above, were explicitly designed not to alter the mass flux calculations, and intervene only on the rotational component only of the flow in the momentum equations. Other choices, involving alterations to the calculation for the divergent flow, would have been possible. However, we judged exact mass conservation more important for climate simulations than exact

287 vorticity conservation. The AM modifications also change the kinetic energy of the flow, and
288 thus change the total energy budget of the model. However, the unmodified FV scheme does not
289 conserve energy. CAM-FV therefore employs an energy “fixer” (analogous to our AM fixer), de-
290 scribed e.g. in Williamson et al. (2015). The fixer diagnoses the energy non-conservation at each
291 time-step. This allowed us to monitor the impact of the AM mods on energy non-conservation
292 in all our experiments. We found no systematic effect, either in sign or in magnitude, of the AM
293 modifications on the energy non-conservation of the model.

294 **3 Numerical Simulations and Results**

295 **3.1 Dry baroclinic wave tests**

296 Initial tests were carried out for adiabatic dynamics and flat bottom topography, from baro-
297 clinically unstable initial conditions as defined in Jablonowsky and Williamson (2006; “JW06”).
298 Figure 3 shows the result in terms of conservation of global AM for CAM-FV integrations at
299 f19 resolution (1.9×2.5 degree of latitude and longitude) and 30 hybrid levels.

300 It may be seen that both the correction and the fixer are effective in reducing the systematic
301 numerical sink of AM in these integrations. In particular, the fixer appears to remove it almost
302 completely; in other words, the integration with the fixer conserves global AM in the time
303 mean. This result is central to this paper, and it proves its two main conclusions. The first is
304 that the systematic non-conservation of global AM in the FV dynamical core indeed resides in
305 the advective wind increments of the shallow-water part of the dynamical core. The second is
306 that, by virtue of its effectiveness, and its formulation that is entirely independent of the model
307 configuration or parametrisations (topography, physical momentum sources, etc), the fixer is a
308 useful and accurate general diagnostic tool that allows us to quantify the numerical torque in any
309 CAM-FV integration. By virtue of this quality, the diagnosed time-averaged fixer tendencies
310 were for example used for the perturbations in the experiments shown in Figures 2 and S2.

311 The impact of the correction on conservation is generally smaller, and different dynamical
312 regimes may be seen when the size and quality of that impact changes. In the baroclinic
313 instability tests of Figure 3, the correction achieves good results in the linear and non-linear
314 stages of baroclinic growth (up to day 30; cf JW06), but is not able to correct the slow drift that
315 sets in after zonalisation of the global flow, then wind speed decreases everywhere as a result of
316 numerical dissipation (there are no external sources or sinks of either momentum or energy in
317 these adiabatic simulations). This is a partly desirable behaviour, as the action of the correction

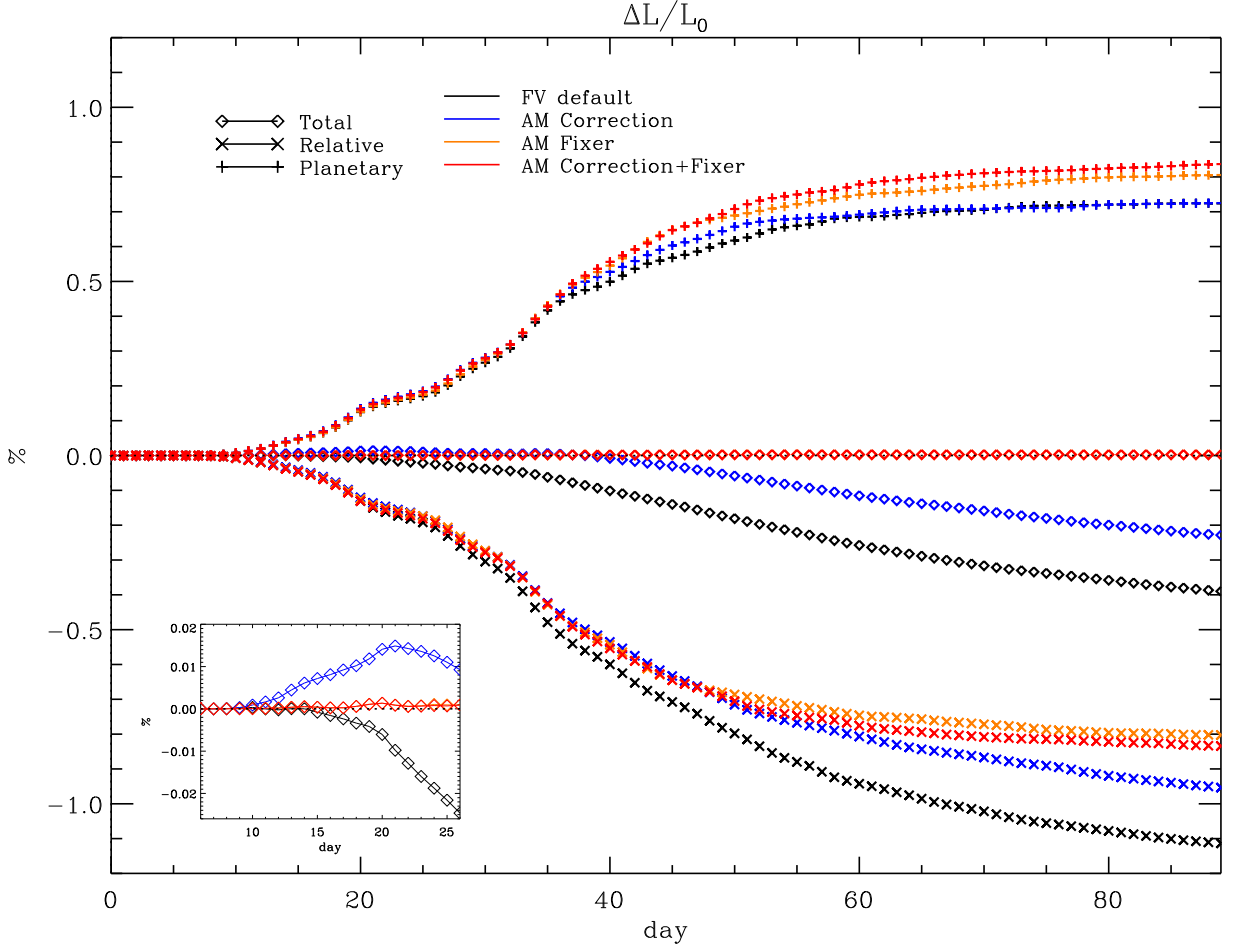


Figure 3: AM correction and fixer in adiabatic, frictionless baroclinic wave tests. Three sets of curves are shown for each of four different simulations with CAM FV, indicating the time evolution of global AM (diamond shapes) and its two components of planetary AM (vertical crosses) and relative AM (x-crosses) in each simulation. Total AM and each AM component are normalised to the initial total AM of the initial state, and differences with respect to initial values are shown, expressed in percentage. Standard CAM-FV is shown in black, CAM-FV with the AM correction only in blue, CAM-FV with the AM fixer only in yellow, and CAM-FV with both AM correction and fixer in red. The inset panel on the lower right of the Figure shows an enlargement for the initial evolution of total AM. Note that the four simulations are nearly indistinguishable before day 8, i.e. during the linear phase of the baroclinic wave. All simulations are run on the two-degree grid.

318 should not change the dissipation properties of the scheme.

319 Aside from the conservation properties they are designed for, both the correction and the
 320 fixer represent a perturbation of the numerical solutions of the FV dynamical core. By arbi-
 321 trarily modifying the relative vorticity associated with the zonal wind, both destroy one of the
 322 fundamental numerical properties of the LR97 formulation, viz. the conservation of absolute

323 vorticity under advection. (In the case of the fixer, the vorticity input has a rigid dependency
324 on latitude, $\sin\varphi$). Figure 4a shows their impact on the accuracy of the JW06 baroclinic wave
325 test in terms of root-mean-square (RMS) of the differences in surface pressure from a nominal
326 reference solution with original FV dynamical core. The latter is obtained for a resolution of
327 $0.9^\circ \times 1.25^\circ$, which is sufficiently close to JW06's reference solution (cf JW06, Section 5(e),
328 points (i) and (ii)) for our purposes. It may be seen that on this measure the solutions with and
329 without the AM corrections are virtually indistinguishable during the stages of both linear and
330 nonlinear baroclinic growth. A similar result holds for the phase (not shown).

331 It may be noted that the largest impact on the RMS of surface pressure arises from the
332 correction. Within the first 30 days this impact is formally always well below significance (as
333 defined in JW06, cf their Figure 10), but it increases in time and eventually becomes appreciable
334 as a full global meridional circulation is established. Similar results hold for the vorticity field,
335 as seen in Figure 4b).

336 Other aspects of the solution besides RMS differences also show limited sensitivity to the
337 application of the correction and the fixer. Figure 5 shows the evolution of the minimum pressure
338 in the developing baroclinic wave. By this measure, the solutions only start to diverge with the
339 filling of the primary cyclone and the deepening of the secondary wave after day 17. The solution
340 with the fixer deepens the secondary cyclone more quickly so that the minimum pressure is seen
341 to jump from first to the second wave minimum between days 18 and 19; this occurs one day
342 later with the unmodified dynamical core. A third transition after day 25 has higher central
343 pressure in the solutions with the fixer; by this time, however, rapid cyclogenesis is occurring
344 in the jet stream of the southern hemisphere, attaining a similar minimum pressure, which is
345 slightly deeper in the solutions with the fixer. In any case the pressure differences of the minima
346 remain of the order of a few hPa, and there is no systematic difference in their position.

347 **3.2 Other idealised tests**

348 Even if the impacts of the modifications of the FV dynamical core are relatively small on local
349 circulations over subseasonal time-scales, as shown above, the rationale for introducing them is
350 the hope of achieving a better simulation of the state of the atmosphere in integrations under
351 specified forcings. As explained in the introduction, one particular expectation is that the
352 subtropical easterlies should weaken, without affecting the circulation elsewhere too heavily. In
353 particular the role of the correction, which alone does not ensure AM conservation, must be

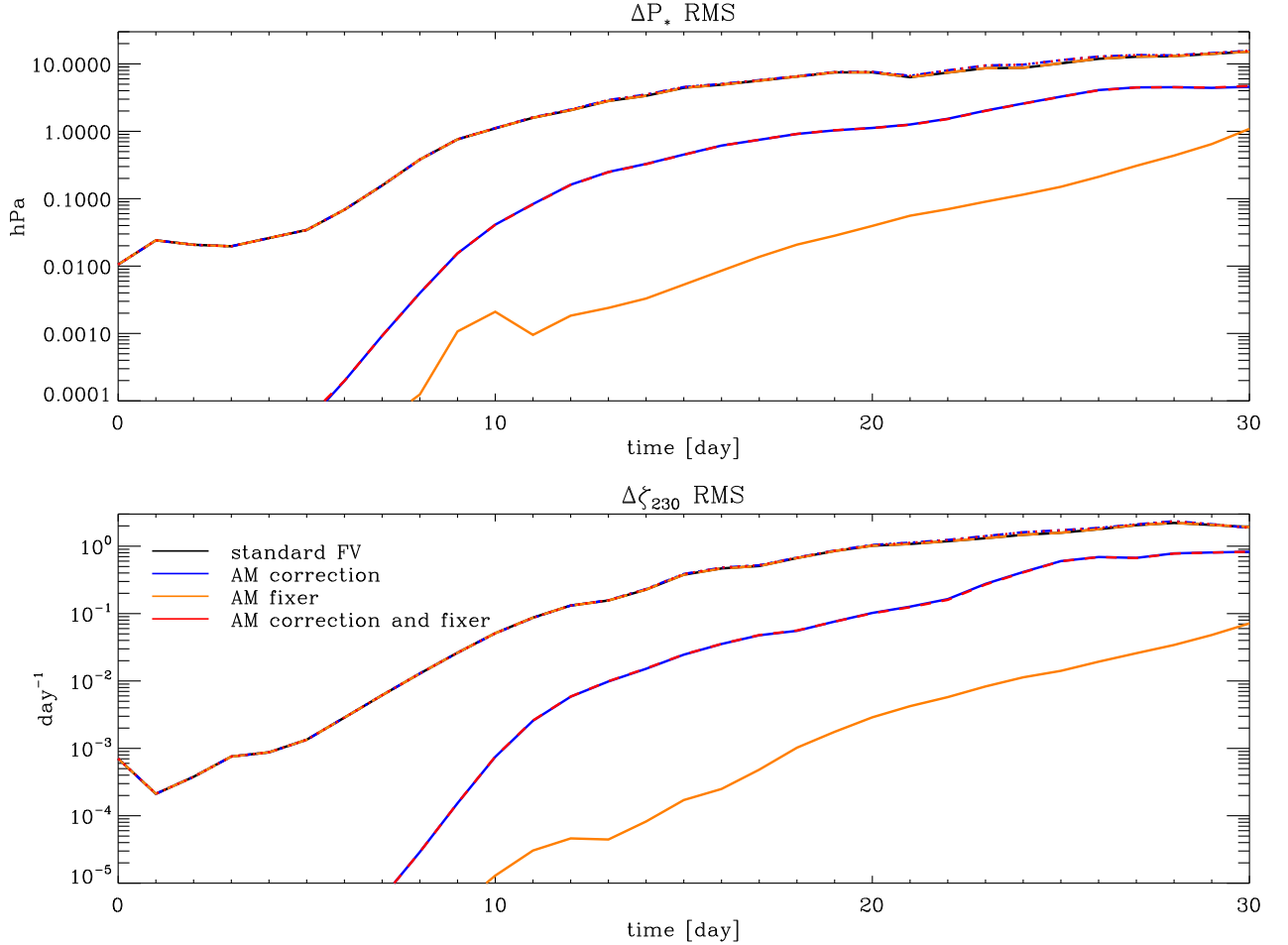


Figure 4: AM correction and fixer in adiabatic, frictionless baroclinic wave test. The simulations shown in Figure 3 are compared with a standard CAM-FV simulation at one degree resolution, and against each other. Each panel shows seven curves, four of which nearly overlap and form the top-most set of lines (including the reference simulation with standard FV). These represent the time evolution of the RMS difference of surface pressure (top panel) and relative vorticity at 230hPa (bottom panel) of each of the two-degree integrations and the control one-degree integration. Below that set of curves are two nearly overlapping curves, which show the RMS differences of the two-degree experiments with AM correction only and the control two-degree integration (blue lines), and of the experiment with both AM correction and fixer and the control integration (red lines). Finally, the single yellow lines at the bottom in each panel show the RMS differences of the two-degree integration with AM fixer only with the two-degree control integration.

354 clarified, and its eventual use justified. Here we document the results of two sets of idealised
 355 simulations that still have a simplified, equipotential lower boundary, but include non-vanishing
 356 physical torques and heating tendencies.

357 The first set of such simulations adhere to the benchmark test of Held and Suarez (1994;

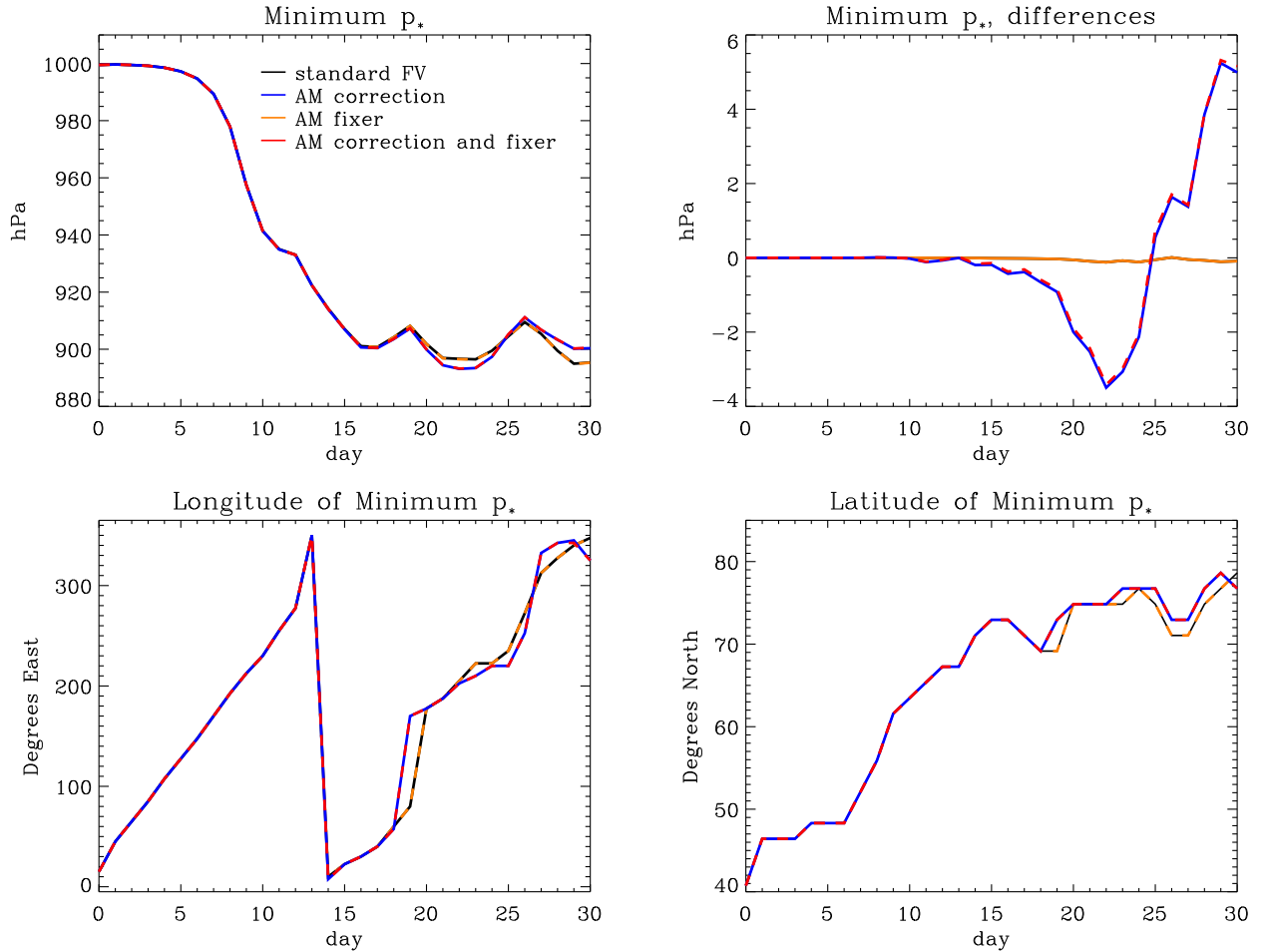


Figure 5: AM correction and fixer in adiabatic, frictionless baroclinic wave test. Evolution of minimum pressure (panel on the top-left) and its position (panels at the bottom) in the baroclinic-wave evolution from the integrations shown in Figure 3. Colour-coding of the lines is the same as in Figure 3. The panel on the top-right shows the differences in minimum pressure between the AM experiments and FV control, with the same colour coding as in the lower curves in Figure 4.

358 “HS” henceforth), where the forcing has the form of a relaxation towards a specified three-
 359 dimensional atmospheric temperature field. Likewise, surface friction is represented by a damp-
 360 ing of the winds within a set of levels near the bottom boundary. Apart from the small numerical
 361 diffusion, these stresses are communicated to the rest of the atmosphere by means of momen-
 362 tum advection in the mean circulation, and of pressure fluctuation in resolved transient motions
 363 (including travelling waves). The second set of simulations follows the Aquaplanet (“AP”) test
 364 first proposed by Neale and Hoskins (2000), where only a persistent field of bottom-boundary
 365 temperatures is prescribed (the “QOBS” profile of Neale and Hoskins 2000), and the full set of

366 moist atmospheric physical parametrisations of CAM6 are used to force the circulation (except
367 for those specific to orographic processes). The bottom boundary is a notional static ocean with
368 unlimited heat and water capacity. Surface stresses are computed by the coupler, and passed
369 to the moist atmospheric boundary-layer parametrisation which then distributes those stresses
370 vertically. Momentum is also transported in moist convection, where active, and further adjust-
371 ments are made when the moist mass of the atmospheric column changes due to precipitation
372 and surface evaporation processes. To simplify the analysis, the gravity-wave parametrisation
373 of CAM6 was turned off in our AP tests. In both sets of tests, FV’s advection scheme is used
374 at PPM’s standard fourth-order at all levels, i.e. the numerical diffusion obtained in standard
375 CAM-FV integrations by employing low-order calculations near the model top is avoided. For
376 initial conditions, HS simulations are cold-started with uniform surface pressure and geopo-
377 tential, and vanishing wind fields except for a westerly perturbation identical to that used in
378 the dry baroclinic wave tests (necessary in order to break zonal symmetry and to allow a non-
379 vanishing correction). The AP simulations all take the same instantaneous atmospheric state
380 from a previous spun-up run, even though this requires more adjustment for the corrected/fixed
381 simulations than for the control.

382 Figure 6a indicates that the global AM conservation properties of the simulations in these
383 tests are broadly in line with the expectations from the previous discussion. Standard FV tests
384 (black lines) show a steady loss of AM in the atmospheric circulation, of a magnitude of the
385 order of 10-20% of the physical flux of AM through the atmosphere. (We count eastward stress
386 as positive, by which the atmosphere gains westerly momentum in the tropical surface easterlies,
387 and loses westerly momentum in the subtropical surface westerlies). Use of the correction leads
388 to an order-of-magnitude reduction of the numerical sink of AM in HS integrations, but it is
389 of limited effectiveness in full-physics AP integrations (blue lines). Integrations with the fixer,
390 with or without the correction (orange and red lines, respectively), maintain atmospheric AM
391 in the time mean. In HS simulations, there appears to be a very small residual drift of AM
392 notwithstanding the fixer. This is due to a small inconsistency in the application of the stress
393 terms, which are calculated and diagnosed in the “physics” part of the model time-stepping,
394 but applied later as velocity tendencies in the physics-dynamics interface on updated layer
395 masses. This is an intrinsic feature of the time-stepping of CAM-FV that we have not modified.
396 More notably, AP simulations differ from HS simulations in that they show obvious fluctuations
397 of total AM around the time mean or around the long-term drift, when there is one. Such
398 fluctuations are similar in all AP integrations, with a magnitude of a few percent of the physical

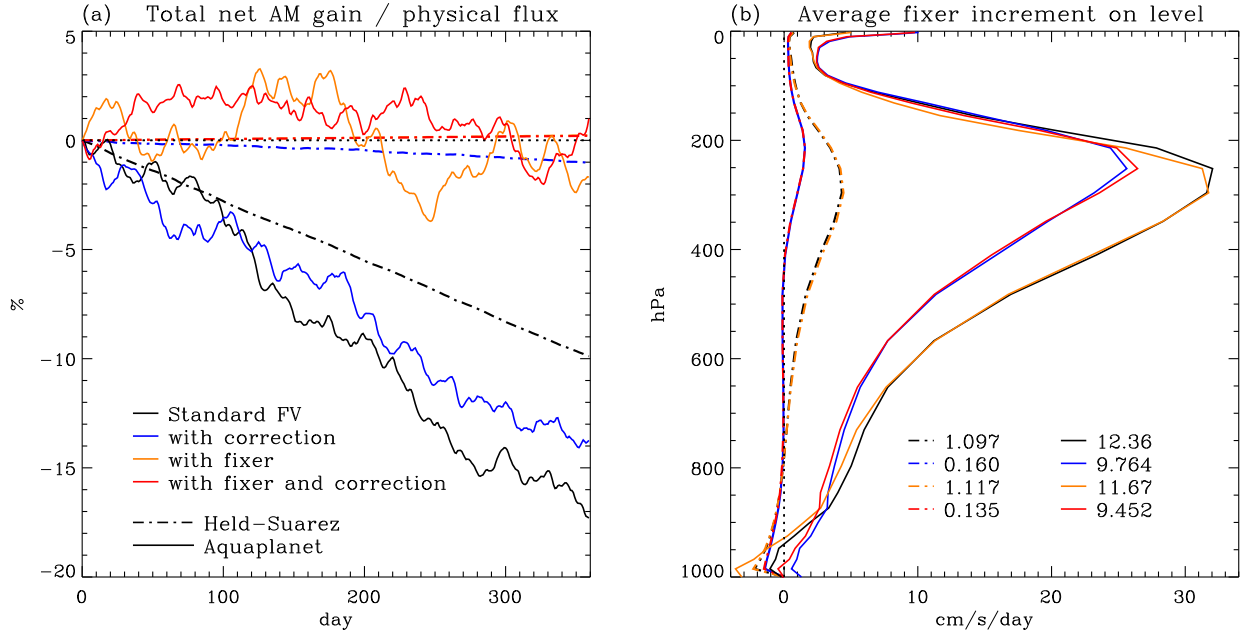


Figure 6: AM correction and fixer in Held-Suarez (HS) and Aquaplanet (AP) integrations. Panel (a) shows the time evolution of total AM for each of the integrations, similar to Figure 3 (diamond shapes) but normalised, separately for each integration, to the time-integrated physical (i.e. surface stress) torque at day 360. AP integrations are shown in solid, HS integrations in stippled lines. The colour coding is as in Figure 3. Panel (b) shows the time-mean numerical torque, averaged over days 120-360, arising at each model level from advective increments, as diagnosed by the fixer, and expressed as equatorial acceleration in a solid-body rotation required to compensate for the numerical sink. Line types and colours correspond to those shown in panel (a). The lists at the bottom of panel (b) indicate the time-mean equatorial accelerations of a *global* solid-body rotation, i.e. the increments shown by the lines but integrated vertically level by level, weighted with the appropriate moments of inertia.

399 sources, and depend on non-conservation in CAM’s physics parametrisations. Fortunately, they
 400 are not systematic and do not produce a noticeable long-term drift.

401 The effectiveness of the fixer in removing most of the AM drift confirms that the systematic
 402 sink of AM in CAM-FV integrations arises predominantly from the shallow-water advection
 403 calculations. The accuracy of the correction, by contrast, depends on the features of the cir-
 404 culation, with good accuracy for numerically well-resolved features, as in the HS tests, but a
 405 poorer one when grid-scale forcing associated with the water cycle occurs. Figure 6b gives more
 406 details on the effect of the correction. Here, the time-average AM sink due to the dynamical
 407 core is diagnosed using the fixer increments for the zonal velocity at the equator at each model
 408 level. This diagnostic is produced irrespective of whether such increments are applied during
 409 the integration. Apart from the smaller increments in HS integrations than in AP integrations,

410 which partly depend on the slower circulation (“surface” stresses are one order of magnitude
411 larger in the HS set-up than in the AP set-up), the advective AM sink has a distinctive shape in
412 pressure-level space, with a maximum in the upper troposphere and small values in the atmo-
413 spheric boundary layer. This shape partly reflects the underlying global-mean zonal wind field,
414 but the maximum sink lies below the maximum wind (at around 250 hPa rather than around
415 150 hPa). The profile of the impact of the correction, i.e. the reduction in fixer increments
416 when the correction is applied, has again a similar shape but with an even lower position of the
417 maximum, which better corresponds with the maximum in the vertical profile of level-integral
418 zonal momentum of the underlying flow. Combined with the off-line diagnostic information for
419 the apparent AM sink from Figure 1, it can be deduced that the main loci of the time-mean
420 AM sink in these simulations are found near the subtropical jet streams, where large zonal
421 asymmetries occur in both the mass fields and the wind fields.

422 The effect on the mean circulation of applying the correction and/or the fixer are shown in
423 Figures 7 and 8 for HS and AP simulations, respectively. The zonal-mean zonal winds are shown,
424 which is the quantity that both the correction and the fixer directly modify. Nevertheless, it
425 should be remembered that the net effect is indirect, since the zonal winds remain in the time-
426 average close to geostrophic balance with the (equivalent) temperature field. In HS simulations,
427 the local temperature differences between simulations are simply proportional to the difference
428 in temperature advection by the meridional and vertical circulation, which is modified primarily
429 through a “tea leaves” mechanism. As already seen in the Introduction, the leading-order effect
430 of the fixer is a weakening of this circulation, and thus of the associated advective temperature
431 tendencies. These tend to cool the lower troposphere in the subtropical easterlies, cool the upper
432 troposphere near the equator, and warm the troposphere poleward of the jet streams. The effect
433 of the fixer on the zonal-mean zonal wind shown in Figure 7a is generally consistent with this
434 expectation, with an equatorward retreat of the surface easterlies and weaker westerlies in the
435 higher latitudes. There is, however, an additional large westerly difference near the equatorial
436 tropopause, which is a direct consequence of the westerly forcing of the fixer, which is greatest
437 at the Equator. This is clearly an undesirable effect of the fixer on the simulations. A more
438 selective effect on the circulation is produced by the correction (Figure 7b). As seen above, its
439 main action is in where the greatest sink of AM is located, i.e. on the flanks of the subtropical
440 jet stream. By correcting part of the AM non-conservation, it also acts to limit the action of
441 the fixer (Figure 7d). As a result, the combination of correction and fixer together, as well
442 as ensuring good global AM conservation, is less severe in terms of its upper-level equatorial

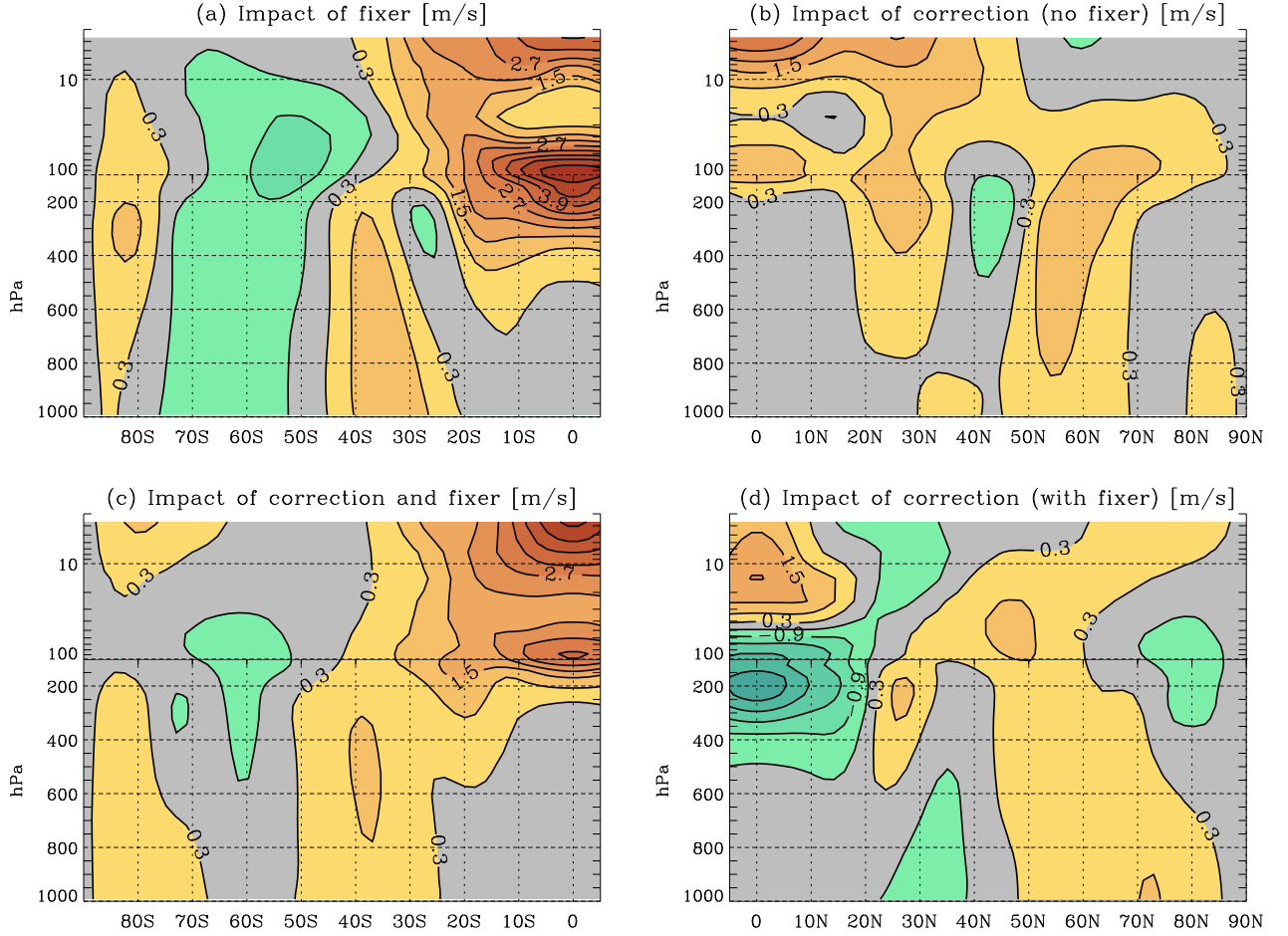


Figure 7: Impact of AM correction and fixer in Held-Suarez simulations. Time-mean latitude-pressure profiles of wind differences between HS simulations shown in the stippled lines in Figure 6. Panel (a) shows the zonal-mean zonal-wind time-average (days 120-360) difference field of the integration with AM fixer only and the control integration. Panel (b) shows the same field, but for the difference between the integration with AM correction and control. Panel (c) shows the difference between the integration with both AM correction and AM fixer and control, and panel (d) that between the integration with both AM correction and AM fixer and the integration with AM fixer only. The contour interval is 0.6 m/s, with blue hues indicating negative values, and red hues positive values. Values in the interval $[-0.3, +0.3]$ m/s are left in grey. The fields displayed have been symmetrised about the equator, since departures from symmetry are very small in the time mean for these hemispherically symmetric simulations. Accordingly, only one hemisphere, and the equatorial region, are shown in each panel.

443 westerly effect (Figure 7d). This suggests that the fixer is best employed in combination with
 444 the correction.

445 In AP simulations, a slow-down of the meridional circulation is still expected and found,
 446 but the interaction between dynamical forcing by the fixer or the correction and the physics

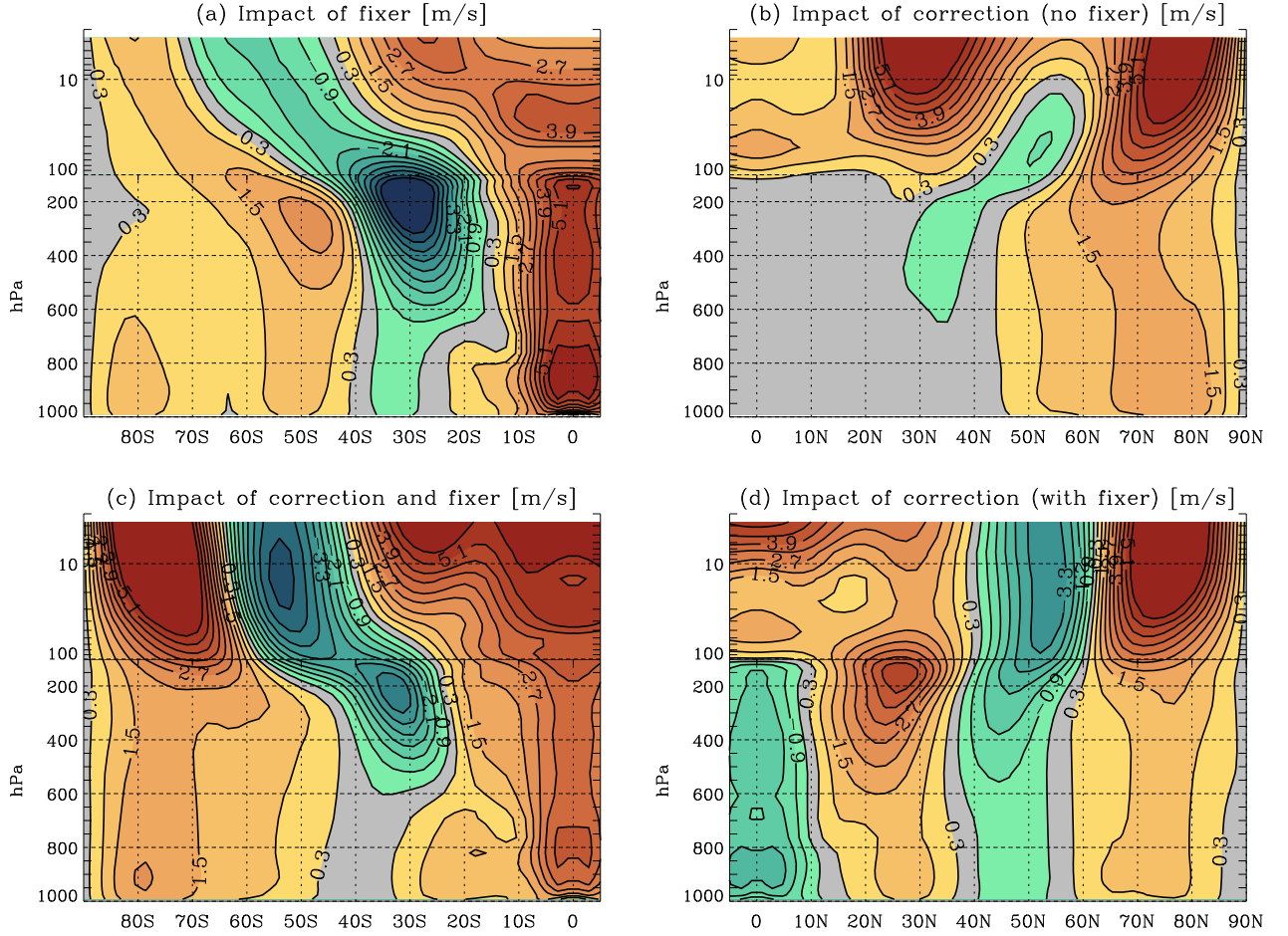


Figure 8: Impact of AM correction and fixer in Aquaplanet simulations. Same as Figure 7, but for the AP simulations shown in the solid lines in Figure 6.

447 tendencies is much more complex and difficult to predict. The fixer now produces large westerly
 448 differences near the equator at all levels, and a marked weakening of the subtropical jet stream
 449 (Figure 8a). The equatorial winds above 300hPa become westerly. The correction is less effective
 450 overall than in HS simulations, and its impacts are mostly confined to levels close to the model
 451 lid or to the high latitudes (Figure 8b). Nonetheless, its use is still beneficial in terms of limiting
 452 the action of the fixer, at least in the troposphere (Figure 8d). The result of the combined
 453 correction and fixer can be seen in Figure 8c. In terms of tropospheric impacts, it appears
 454 acceptable; equatorial winds remain easterly below 200hPa, and weak above. The weakening
 455 of the equatorial and tropical easterlies compared with the control simulation implies greater
 456 similarity with simulations with AM-conserving spectral models. Large changes however can
 457 be seen near the model lid, especially in the four model layers with pressures less than 25

458 hPa. This is a consequence of momentum accumulation within these layers. In CAM’s default
459 configuration, the order of FV’s PPM advection scheme is reduced here, which results in large
460 numerical dissipation. Effectively, these levels are used as sponge layers and are thus not part of
461 the valid computational domain of the model. In full-model configurations it is therefore advised
462 to keep the reduced order of advection and turn off both the correction and the fixer in these
463 layers. The large mean-state changes seen near the top in Figure 8d then vanish. Considering
464 the troposphere only, the conclusion obtained from HS simulations can be seen to hold also
465 for full-physics AP model simulations, in that the combined application of the fixer and the
466 correction results in smaller overall mean-state changes of the solution compared to default FV
467 without modifications, while ensuring good conservation of AM.

468 4 Simulations of the observed climatology

469 The relevance of the AM modifications to the FV dynamical core for CAM simulations in realistic
470 configuration is investigated here using “F2000” cases, which are AMIP-type simulations (Gates
471 1992) where SSTs and all compositional forcings are prescribed as a repeating annual cycle
472 obtained from an observed climatology of the decade spanning the turn of the century. We
473 test at two grid resolutions, one of $1.9^\circ \times 2.5^\circ$ (“f19”) as in all integrations already discussed
474 above, and one of $0.9^\circ \times 1.25^\circ$ (“f09”), to test the impacts of AM modifications in a case that is
475 scientifically supported by NCAR at this time. The CESM model version used (here as above)
476 is release 2.1.1¹

477 Figure 9 illustrates the effects of the fixer and the correction on f19 simulations. The control
478 simulation shows a characteristic easterly surface wind-stress bias throughout the Tropics (Figure
479 9a). In addition, there are excessive westerlies at southern high latitudes. The effect of the fixer
480 is to reduce the tropical biases (Figure 9b), with an evident westerly effect on the simulations
481 nearly symmetrically about the equator (Figure 9d). By that same token, however, the high-
482 latitude westerly errors are enhanced (Figure 9b). The application of the correction in addition
483 to the fixer not only brings further improvements in the tropics, but also corrects the westerly
484 effect of the fixer in high latitudes (Figure 9e). The result is a significant improvement in the
485 simulation of the surface wind-stress field over the entire ocean domain.

¹More precisely, we used a pre-release of CESM2.1.1 (#20, 22 March 2019). In terms of the simulations presented in this paper, the differences with the full 2.1.1 release only affect the F2000 cases at f19 resolution, where slightly different emission datasets are used to force the simulations. The impacts of this are of negligible consequence for the results discussed in this Section.

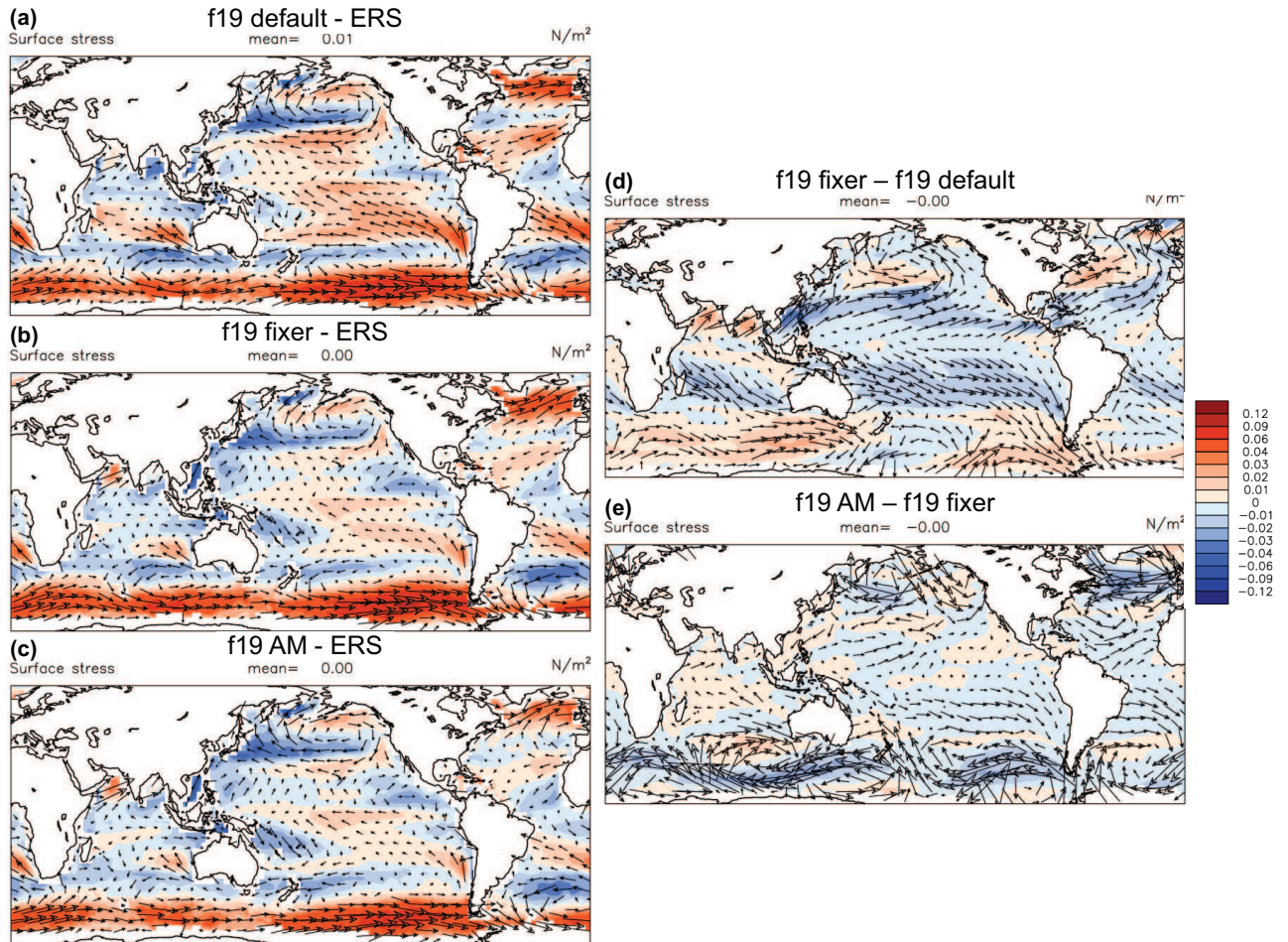


Figure 9: Impact of AM correction and fixer in F2000 simulations. Panels (a), (b) and (c) show maps of surface wind-stress vector differences (arrows) and wind-stress magnitude differences (colours) between “F2000” simulations with CAM-FV at $1.9^{\circ} \times 2.5^{\circ}$ degree resolution (“f19”) and a climatology obtained from satellite scatterometer observations (ERS; Quilfen et al. 1999). Panel (a) shows the annual-mean climatological bias in the f19 control integration; panel (b) for a f19 simulation with AM fixer only; and panel (c) for an f19 simulations with both AM correction and AM fixer. Panels (d) and (e) show the same fields, but for the differences between the simulation with fixer only and control, and between the simulation with both fixer and correction and that with fixer only. The colour scale for all plots is on the right of panels (d) and (e). These plots were produced with the AMWG diagnostics package developed by the Atmospheric Model Working Group of the University Corporation for Atmospheric Research and the National Center for Atmospheric Research.

486 In general, we obtain a similar conclusions as for the AP simulations. The impact of the
 487 correction on the global conservation of AM is modest, removing only about 15% of the sink at
 488 f19 resolution. However, its action is stronger on upper-level winds (cf. Figure 6b), which leads
 489 to proportionally reduced fixer increments at those levels, and thus to smaller impacts by the

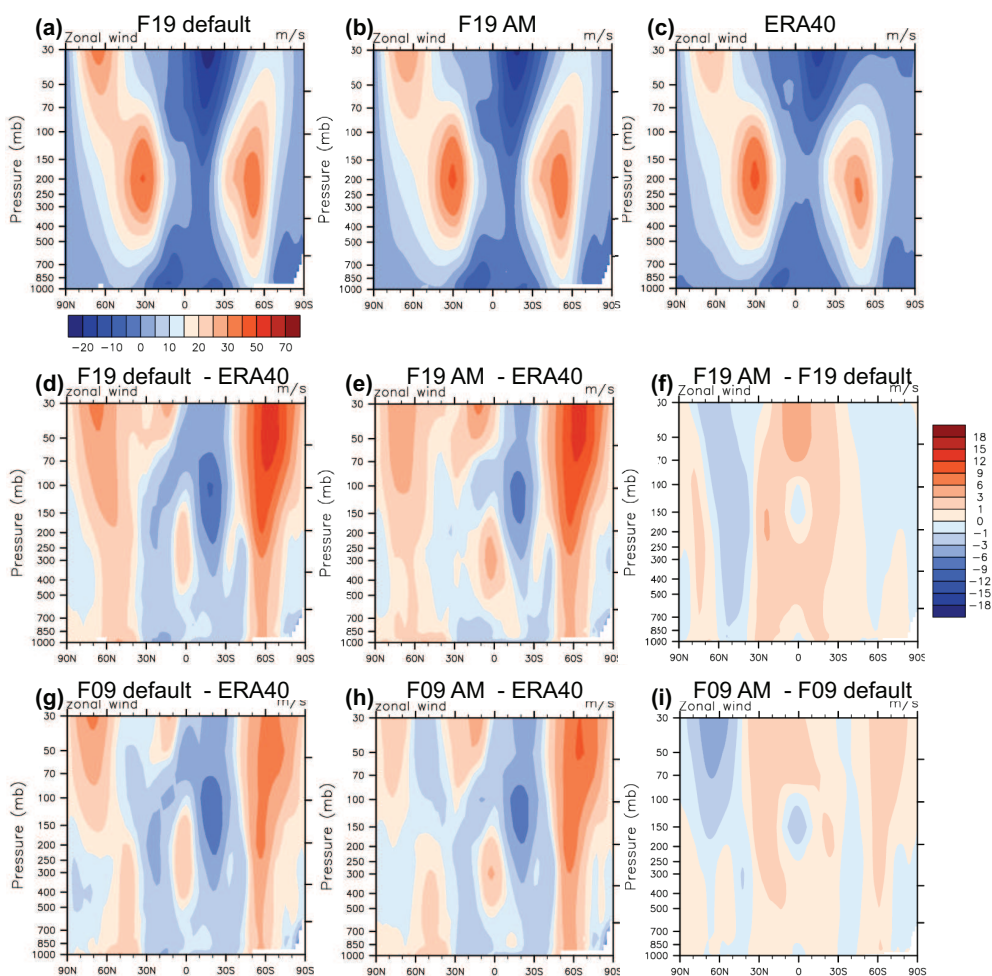


Figure 10: Impact of AM correction and fixer in F2000 simulations. Latitude-pressure maps of zonal-mean zonal wind climatologies for boreal winter (DJF). Panels (a), (b) and (c) show total fields for the CAM-FV f19 control simulation, (panel (a)) for the f19 simulation with both AM fixer and AM correction (panel (b)), and for the ERA40 reanalysis (Uppala et al., 2005). The colour scale is at the bottom of panel (a). Panels (d) and (e) show the differences of each of the two f19 integrations and ERA40, and panel (f) shows the differences between the two f19 simulations. The colour scale is on the right of Panel (f). Panels (g), (h), and (i) are analogous to panels (d), (e), and (f), respectively, but for CAM-FV simulations at $0.9^\circ \times 1.25^\circ$ resolution. These plots were produced with the AMWG diagnostics package developed by the Atmospheric Model Working Group of the University Corporation for Atmospheric Research and the National Center for Atmospheric Research.

490 fixer on areas affected by baroclinic instability.

491 Figure 10 and Figure S3 in the supplementary information shows the seasonally resolved
 492 impacts on the zonal-mean zonal winds from applying the combination of fixer and correction
 493 in F2000 simulations at both f19 and f09 resolutions (cf also Figure S3 in the supplementary

494 information, for JJA). In all cases, the reduction of biases in both easterly and westerly wind
495 regimes is noticeable, the latter especially at the sub-polar latitudes of the winter hemisphere.

496 More in detail, it may be noted that the benefits of the AM modifications appear more
497 clearly for the winds in the simulation at the lower resolution, where the numerical sink of AM
498 is indeed larger. These benefits however are not limited to the zonal-mean zonal winds, and
499 they are also appreciable at the f09 resolution. Most notable is the reduction in the strength
500 of the Hadley circulations (cf Figure S4 in the Supplementary Information), which is expected
501 from the arguments set out in the Introduction. This has consequences for many aspects of the
502 global circulation. Figure 11 shows a summary of the impacts on the quality of the simulations
503 in relation to the observed climatology. The improvements at f09 seems particularly remarkable
504 considering that the unmodified simulation is a scientifically supported case that has been fully
505 tuned for a best match to observations. It may be noted that no additional tuning whatsoever
506 is involved in the simulation with AM modifications shown here, and that the AM modifications
507 themselves have no free parameters as they follow directly from an effort to reduce the numerical
508 sink stemming from the FV dynamical core. The better quality of this simulation thus follows
509 entirely from better adherence of the solution to a fundamental property of the equations of
510 motion. Indeed, it should be kept in mind that the AM modification of the FV dycore

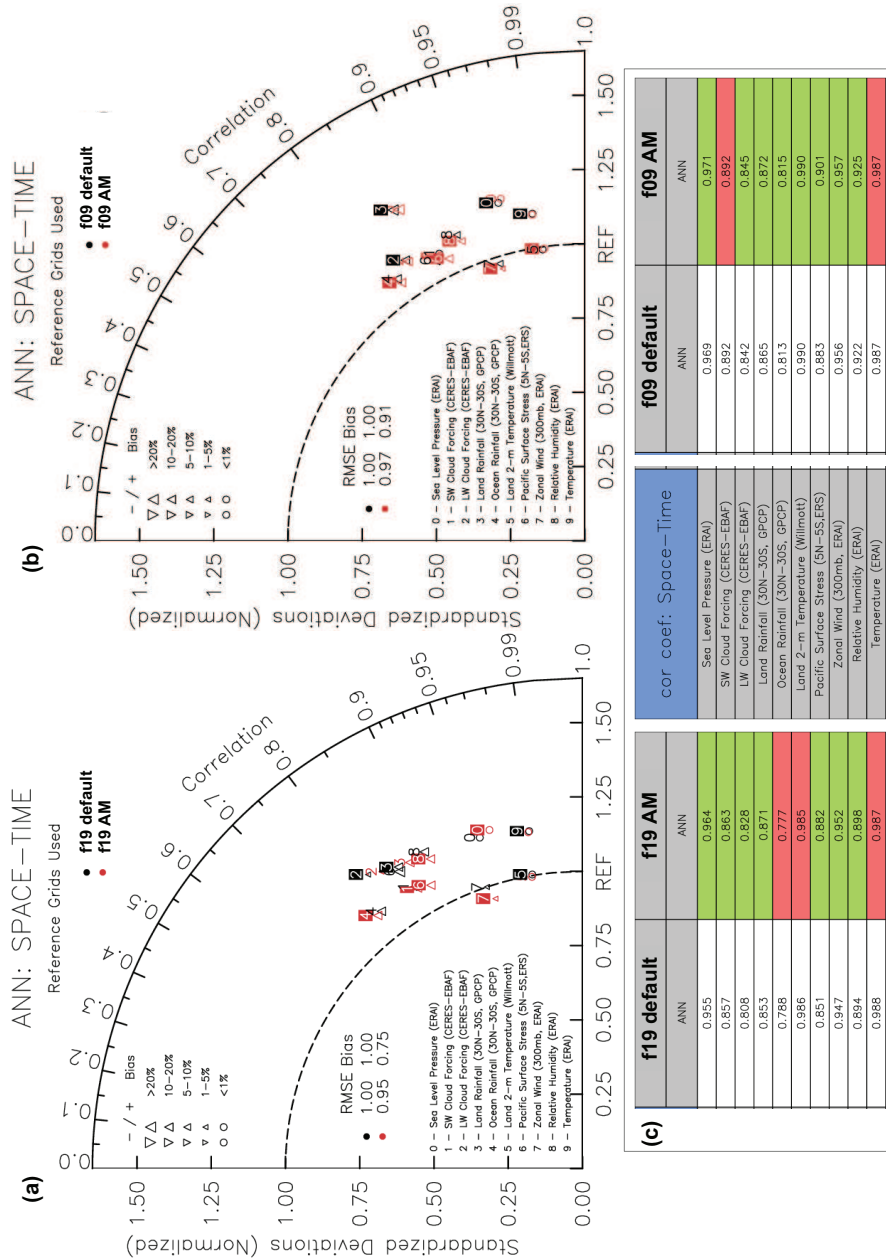


Figure 11: Impact of AM correction and fixer in F2000 simulations. Panels (a) and (b) show Taylor (2001) diagrams for the validation of the CAM-FV “F2000” simulations at f19 (panel (a)) and at f09 (panel (b)) resolution against observations for a standard set of diagnostic fields, listed in the panels. Black symbols represent RMS differences to observations for the control simulations without modifications, and red symbols for the simulations using both the AM correction and the AM fixer. For the overall RMSE and bias scores, those from the control simulations are used as normalisation. Panel (c) summarises the correlation values between simulated and observed diagnostic fields as listed in the central table. Green fields mark all instances where one of the AM-modified simulation represents an improvement over the respective control simulation. These plots were produced with the AMWG diagnostics package developed by the Atmospheric Model Working Group of the University Corporation for Atmospheric Research and the National Center for Atmospheric Research.

Table 1: Simulation set-ups and the effect of AM modifications. The percentage figures represent the numerical source (negative for sink) of global total atmospheric AM relative to the global total physical eastward torque acting on the atmosphere (terms T_x and C_λ in Eq.(A1, when only the positive part of the integrands are summed). The column “Experiments” indicate which modification to CAM-FV are used (the relevant sections of this paper are indicated in the footnotes). The three columns under “Simulations” are for results obtained with model integrations in Held-Suarez mode (Held and Suarez, 1994), in aquaplanet mode (Neale and Hoskins, 2000), and in “F2000” mode, i.e. an AMIP-type (Gates 1992) simulation with annually repeating present-day climatological SSTs.

Experiments	Simulations ($f19, 1.9^\circ \times 2.5^\circ$)		
	HS	AP	F2000
geometry and pressure only ¹	-7.1%	-23.8%	-26.5%
AM correction ²	0.3%	-19.8%	-24.7%
AM correction and fixer ³	0.7%	1.9%	0.8%

¹Sections 2.2 and 2.1

²Section 2.3

³Section 2.3 and Section 2.4

511 5 Summary and Conclusions

512 AM conservation in CAM-FV has been substantially improved by means of a correction that
513 reduces the zonal-mean numerical sink of Lin and Rood’s (1997) shallow-water scheme, and a
514 fixer that ensures conservation of global angular momentum under advection. The effective-
515 ness of these modification in terms of AM conservation in the simulations presented here is
516 summarised in Table 1. We show that aside from global AM conservation, they have other sig-
517 nificant impacts on the simulations, consistent with the “tea-leaves” mechanism (Einstein 1926)
518 that rapidly redistributes pressure forces in a rotating fluid in response to zonal accelerations.
519 The most notable effect is a reduction of the excessive easterlies of the model, with a concomi-
520 tant slow-down of the Hadley circulation. As a result of such changes, the simulations of the
521 observed climatology shows marked improvements.

522 The zonal-mean correction of the shallow-water scheme is not necessary for enforcing global
523 conservation, as this can be achieved by the fixer alone. Indeed, the correction is quite ineffective

524 in realistic simulations of the atmosphere in terms of global conservation. Nevertheless, we
525 find that its concomitant application with the fixer has positive impacts on the simulations.
526 In particular, it reduces the effects of the fixer in the mid-latitudes. This can be explained
527 with the greater effectiveness of the correction in the baroclinically unstable regions around
528 the subtropical jet streams, where the zonal-mean numerical sink appears to be largest. Even
529 so, because of its potentially large local effects, the utilisation of the correction under different
530 set-ups should be tested on a case-by-case basis according to its impacts on the results.

531 Improving the quality of the simulation of the global distribution of surface wind-stress should
532 be expected to bring particular benefits to coupled atmosphere-ocean simulations. An adequate
533 discussion of such coupled simulation would exceed the scope of the present manuscript, which is
534 aimed primarily at presenting the method. In particular, due to their computational expense, at
535 the present time it is not possible to produce well spun-up coupled simulations that can provide
536 an assessment of the impact of the AM modifications.

537 The modification to the FV dynamical core that we describe and utilise are relatively crude,
538 and cause local loss of accuracy due to violation of vorticity conservation under advection.
539 Nevertheless, the associated detrimental impacts appear to be fairly limited, with insignificant
540 differences under standard tests such as the Jablonowsky and Williamson (2006) baroclinic wave
541 test, which should be sensitive to local conservation. Even so, it is clear from the very same tests
542 that simulations over weather time-scales are not sensitive to AM conservation, so that for such
543 application it is not advisable to trade enforcing such conservation for a loss of accuracy. On the
544 longer time-scales of climate simulations, by contrast, our results demonstrate the importance
545 of global conservation of atmospheric AM in order to obtain a realistic global circulation.

546 **Code and data availability.**

547 The code used in the numerical simulations of this paper is available under

548 <https://zenodo.org/badge/latestdoi/214872045>

549 CAM6 is published in the open-access CESM ESCOMP git repository, freely available under
550 <https://github.com/ESCOMP>. The AM options can be switched on by setting standard CAM
551 namelist parameters to non-default values (i.e. T instead of F; there are no free numerical
552 parameters). Apart from these switches, all atmosphere model configurations presented in this
553 paper are standard CESM cases that can be set up and run using the scripts provided in the
554 repository. Users can obtain technical support if requested.

555 **Author Contributions:** Thomas Toniazzo conceived the idea, proposed the work, made the
556 calculations, implemented the code, ran the simulations, evaluated them, produced all figures,
557 and wrote the manuscript. Mats Bentsen supported this activity through national infrastructure
558 projects of the Norwegian Research Council. Cheryl Craig, Brian Eaton and James Edwards
559 revised the code and included it in the official ESCOMP CESM repository. Steven Goldhaber
560 gave technical advice on CAM code and simulations. Peter Lauritzen, Mats Bentsen, and
561 Christiane Jablonowski were at hand for critical discussion of the scientific ideas and helped
562 providing the initial impetus of this work. Mats Bentsen, James Edwards, Steve Goldhaber,
563 and Peter Lauritzen also provided useful comment and suggestions on the draft manuscript.

564 **Acknowledgements:** Warm thanks go to Prof. Christoph Heinze for his unbending dedi-
565 cation to model development in the NorESM consortium and allowing in particular this work to
566 go forward. We are grateful to Dr. Alok Gupta at NORCE and Dr. Cecile Hannay at NCAR
567 for their crucial work in carrying out and supporting NorESM and CESM development simu-
568 lations. This work was partially funded by Norwegian Research Council grant #229771 (EVA)
569 and #270061 (INES).

References

570
571 Arakawa, A., and V.R. Lamb, 1981: A potential enstrophy and energy conserving scheme
572 for the shallow water equations. *Mon. Wea. Rev.* 109, 18-36.

573 Blackburn, M., D. L. Williamson, K. Nakajima, W. Ohfuchi, Y. O. Takahashi, Y.-Y.
574 Hayashi, H. Nakamura, M. Ishiwatari, J. L. McGregor, H. Borth, V. Wirth, H. Frank,
575 P. Bechtold, N. P. Wedi, H. Tomita, M. Satoh, M. Zhao, I. M. Held, M. J. Suarez, M.-I.
576 Lee, M. Watanabe, M. Kimoto, Y. Liu, Z. Wang, A. Molod, K. Rajendran, A. Kitoh,
577 and R. Stratton: The Aqua-Planet Experiment (APE): CONTROL SST simulation. *J.*
578 *Meteor. Soc. Japan*, 91A, 17-56, doi:10.2151/jmsj.2013-A02. 2013.

579 Colella, P., and P.R. Woodward: The piecewise parabolic method (PPM) for gas-dynamical
580 simulations. *J Comp Phys* 54 , 174-201. 1984.

581 Egger, J., and K.-P. Hoinka: The annual cycle of the axial angular momentum of the
582 atmosphere. *J. Climate* 18, 757-771. 2005.

583 Einstein, A.: Die Ursache der Mäanderbildung der Flußläufe und des sogenannten Baer-
584 schen Gesetzes. *Die Naturwissenschaften* 11, 223-224. 1926.

585 Feldl, N. and S. Bordoni: Characterizing the Hadley circulation response through regional
586 climate feedbacks. *J. Climate*, 29, 613622, doi:10.1175/JCLI-D-15-0424.1. 2016.

587 Gates, W. L., 1992: AMIP: The Atmospheric Model Intercomparison Project. *Bull. Amer.*
588 *Meteor. Soc.*, 73, 19621970.

589 Hadley, G.: Concerning the cause of the general trade-winds. *Phil. Trans.* 39, 58-62.
590 1735.

591 Held, I.M., and A.Y. Hou: Nonlinear axially symmetric circulations in a nearly inviscid
592 atmosphere. *J. Atmos. Sci.* 37, 515-533. 1980.

593 Held, I. M., and M. J. Suarez: A proposal for the intercomparison of the dynamical cores
594 of atmospheric general circulation models, *Bull. Am. Meteorol. Soc.*, 75, 18251830. 1994.

595 Hollingsworth, A., Killberg, P., Renner, V., and D.M. Burridge: An internal symmetric
596 computational instability. *Q. J. R. Meteorol. Soc.* 109 , 417-428. 1983.

597 Jablonowski, C., and D. L. Williamson: A Baroclinic Instability Test Case for Atmospheric
598 Model Dynamical Cores, *Quart. J. Roy. Met. Soc.*, Vol. 132, 2943-2975. 2006.

599 Quilfen, Y., B. Chapron, A. Bentamy, J. Gourrion, T. Elfouhaily, and D. Vandemark:
600 Global ERS-1/2 and NSCAT observations: Upwind/crosswind and upwind/downwind
601 measurements. *J. Geophys. Res.*, 104, 1145911469. 1999.

602 Laprise, R., and C. Girard: A spectral general circulation model using a piecewise-constant
603 finite-element representation on a hybrid vertical coordinate system. *J. Climate* 3, 32-52.
604 1990.

605 Lauritzen P.H., Bacmeister J.T., Dubos T., Lebonnois S., and M.A. Taylor: Held-Suarez
606 simulations with the community atmosphere model spectral element (CAM-SE) dynamical
607 core: a global axial angular momentum analysis using Eulerian and floating Lagrangean
608 vertical coordinates. *J. Adv. Model. Earth Syst.* 6, 129-140. doi:10.1002/2013MS000268.
609 2014.

610 Lebonnois, S., C. Covey, A. Grossman, H. Parish, G. Schubert, R. Walterscheid, P. H.
611 Lauritzen, and C. Jablonowski: Angular momentum budget in general circulation mod-
612 els of superrotating atmospheres: A critical diagnostic, *J. Geophys. Res.*, 117, E12004,
613 doi:10.1029/2012JE004223. 2012

614 Lin, S.J.: A finite-volume integration method for computing pressure gradient force in
615 general vertical coordinates. *Quart. J. R. Meteorol. Soc.* 123 , 1749-1762. 1997.

616 Lin, S.J., and R.B. Rood: An explicit flux-form semi-Lagrangian shallow-water model on
617 the sphere. *Quart. J. R. Meteorol. Soc.* 123 , 2477-2498. 1997.

618 Lin S.-J.: A “vertically lagrangian” finite-volume dynamical core for global models. *Mon.*
619 *Wea. Rev.* 132, 2293-2307. 2004.

620 Lindzen, R.S., and A.Y. Hou: Hadley circulations for zonally averaged heating centered
621 off the equator. *J. Atmos. Sci.* 45, 2416-2427. 1988.

622 Lipat, B. R., G. Tselioudis, K. M. Grise, and L. M. Polvani: CMIP5 models shortwave
623 cloud radiative response and climate sensitivity linked to the climatological Hadley cell
624 extent, *Geophys. Res. Lett.*, 44, 57395748, doi:10.1002/2017GL073151. 2017

625 Neale, R. B., and B. J. Hoskins: A standard test for AGCMs including their physical
626 parameterizations. II: Results for the Met Office model. *Atmos. Sci. Lett.*, 1, 108114,
627 doi:10.1006/asle.2000.0024. 2000.

628 Pauluis, O.: Boundary layer dynamics and cross-equatorial Hadley circulation. *J. Atmos.*
629 *Sci.* 61, 1161-1173. 2004.

630 Schneider, E.K.: Axially symmetric steady-state models of the basic state for instability
631 and climate studies. Part II: Nonlinear calculations. *J. Atmos. Sci.* 34, 280-297. 1977

632 Simmons, A.J., and D.M. Burridge: An energy and angular-momentum conserving vertical
633 finite-difference scheme and hybrid vertical coordinates. *Mon Wea Rev* 109 , 758-766. 1981.

634 Taylor, K.E.: Summarizing multiple aspects of model performance in a single diagram. *J.*
635 *Geophys. Res.* 106, 7183-7192. 2001.

636 Uppala, S. M., and Coauthors: The ERA-40 Re-Analysis. *Quart. J. Roy. Meteor. Soc.*,
637 131, 29613012. 2005.

638 Walker, C.C., and T. Schneider: Eddy influences on Hadley circulations: simulations with
639 an idealized GCM. *J. Atmos. Sci.* 63, 3333-3350. 2006.

640 White, A.A., Hoskins, B.J., Roulstone, I., and A. Staniforth: Consistent approximate
641 models of the global atmosphere: shallow, deep, hydrostatic, quasi-hydrostatic, and non-
642 hydrostatic. *Quart. J. Roy. Meteorol. Soc.* 131, 2081-2107. 2005.

643 Williamson, D. L., J. G. Olson, C. Hannay, T. Toniazzo, M. Taylor, and V. Yudin (2015),
644 Energy considerations in the Community Atmosphere Model (CAM), *J. Adv. Model.*
645 *Earth Syst.*, 7, 11781188, doi:10.1002/2015MS000448.

A Off-line diagnostics of numerical torque in model simulations

The diagnosis of the residual torque that violates AM conservation in CAM simulations follows from the hydrostatic Primitive Equations (cf. White et al. 2005). In our zonally and vertically integrated diagnostics such as in Figure 1 the AM source is calculated as

$$S_M = \partial_t L_r + D_L - T_x - C_\lambda \quad (\text{A1})$$

where the first term on the r.h.s. represent the tendency of relative atmospheric AM, the second term represent the divergence of the flux of relative AM, the third the external torque (which in all simulations presented in Sections 1, 2, and 3, when non-vanishing, is exclusively due to surface stresses or linear friction in the PBL), and the last term is the tendency of planetary atmospheric AM due to the vertically integrated divergence of atmospheric mass. In formulas:

$$\begin{aligned} L_r &= \int_0^{2\pi} \int_{p_*}^{p_{top}} (ua \cos \varphi) \frac{dp}{g} a \cos \varphi d\lambda \\ D_L &= \frac{1}{a} \frac{\partial}{\partial \varphi} \int_0^{2\pi} \int_{p_*}^{p_{top}} (uva \cos \varphi) \frac{dp}{g} a \cos \varphi d\lambda \\ T_x &= \int_0^{2\pi} (\tau_x a \cos \varphi) a \cos \varphi d\lambda \\ C_\lambda &= -\frac{a\Omega \sin 2\varphi}{g} \partial_t \int_0^{2\pi} \int_0^\varphi p_* a^2 \cos \varphi' d\varphi' d\lambda \quad , \end{aligned}$$

where a is the Earth's radius, φ the latitude, λ the longitude, g the gravitational acceleration in Earth's surface, Ω the angular speed of Earth's rotation, and u , v , p_* and τ_x are the zonal wind component, the meridional wind component, the surface pressure, and the zonal component of the surface or frictional stress acting on the air in the model simulations. Note that to obtain C_λ the continuity equation was used. Note that for the time-average values of S_M , the time differentials become increments between the initial and the final state; terms T_x and C_λ are linear in the wind-stress and the surface pressure, respectively. Terms L_r and D_L are bi- and trilinear in the model prognostic quantities u , v , p_* , so an on-line computation of the time averages of the integrands are required for these terms. CAM provides time-mean diagnostic of the zonal wind u and of the product of the wind components uv conservatively interpolated onto standard pressure levels, and the integrals in Eq.(A1) are computed with their help.

B Formulation and approximations for the AM correction in CAM-FV

The local conservation equation for the shallow-water equations is

$$\begin{aligned} \partial_t [\Delta p (ua \cos \varphi + \Omega a^2 \cos^2 \varphi)] = & \\ & - \frac{1}{a \cos \varphi} \partial_\varphi [\Delta p (ua \cos \varphi + \Omega a^2 \cos^2 \varphi) v \cos \varphi] \\ & - \frac{1}{a \cos \varphi} \partial_\lambda [\Delta p (ua \cos \varphi + \Omega a^2 \cos^2 \varphi) u] , \end{aligned} \quad (\text{A2})$$

where (φ, λ) are latitude and longitude, respectively, Δp is the layer thickness in terms of hydrostatic pressure, (u, v) are the zonal and meridional wind components, a is the Earth's radius, and Ω the Earth's angular velocity. Note that we are ignoring pressure and geopotential terms here, as we focus exclusively on the process of advection. Accordingly, Δp , i.e. the layer under consideration, may be arbitrary, except that it satisfies the shallow-water mass conservation equation, i.e. we follow Lin's (2004) "vertically Lagrangian" approach by following the vertical motion of the layer. Integrating Eq.(A2) over longitude, we obtain:

$$\int d\lambda \partial_t (\Delta p ua \cos^2 \varphi) = - \int d\lambda \partial_\varphi (\Delta p uv \cos^2 \varphi) + \int d\lambda \Delta p fva \cos^2 \varphi , \quad (\text{A3})$$

where f is the Coriolis parameter. To address the FV scheme's violation of this conservation, we apply an additional, zonally uniform increment of the zonal wind, $\overline{\delta u}$, such that, over each shallow-water sub-step δt (we shall refer to this simply as the "time-step" in this section) of the dynamical core:

$$\begin{aligned} \frac{1}{\delta t} \int d\lambda \cos \varphi [\Delta p_n (u_n + \overline{\delta u}) - \Delta p_o u_o] \cos \varphi = & \\ & - \int d\lambda \cos \varphi \frac{1}{a \cos \varphi} \partial_\varphi (\Delta p uv \cos^2 \varphi) \\ & + \int d\lambda \cos^2 \varphi \Delta p f v . \end{aligned} \quad (\text{A4})$$

Here, "old" prognostic quantities (i.e. valid at the beginning of the time-step) and "new" prognostic quantities (i.e. valid at the end of the time-step, before any correction) are indicated by the sub-scripts "o" and "n", respectively; quantities without subscripts are intended as time-centred representing advective fluxes over the time-step. To obtain the correction, we solve this equation for the required increment $\overline{\delta u}$ and substitute for u_n the actual FV zonal wind increment over the time-step:

$$u_n = u_o + \left(\xi_o v - \frac{1}{a \cos \varphi} \partial_\lambda K \right) \delta t , \quad (\text{A5})$$

687 where ξ is the absolute vorticity, and K is the kinetic energy term as discretised in LR97's
 688 scheme. The result is:

$$\begin{aligned}
 \left(\int d\lambda \Delta p_n \right) \overline{\delta u} &= - \int d\lambda \Delta p_n \left(\zeta_o v - \frac{1}{a \cos \varphi} \partial_\lambda K \right) \delta t \\
 &- \int d\lambda (\Delta p_n - \Delta p_o) [u_o + (\xi_o v - \zeta_o v) \delta t] \\
 &- \int d\lambda \frac{1}{a \cos^2 \varphi} \partial_\varphi (\Delta p uv \cos^2 \varphi) \delta t.
 \end{aligned} \tag{A6}$$

689 The term in the second line on the right-hand side representing advection of planetary vorticity
 690 is written in a roundabout way for later convenience.

691 We note two aspects of this expression. First, there is a significant numerical cancellation
 692 between the second and the third lines on the right-hand side. Second, all advective terms in
 693 the first two lines on the right-hand side can be easily discretised according to standard LR97's
 694 prescription, and are thus automatically defined on D-grid u-points, i.e. where required for $\overline{\delta u}$.
 695 However, all mass factors are defined on scalar points, i.e. on the A-grid. Furthermore, the
 696 integrand in the third line on the rhs has no natural expression in LR97's discretisation, and
 697 both zonal and meridional winds in that expression need to be interpolated onto the A-grid.
 698 Hence, additional interpolation is required for these terms. Notwithstanding these issues, we
 699 found that this correction, when implemented, gave accurate conservation of AM. However, it
 700 also proved to cause numerical instability, such that the integration crashed within seven or
 701 eight time-steps. Analysis suggested that the last term on the rhs had to be recast in a different
 702 form.

703 We therefore chose to approximate the last term, as follows:

$$\frac{1}{a \cos^2 \varphi} \partial_\varphi (\Delta p uv \cos^2 \varphi) \approx \left[\frac{1}{a \cos \varphi} \partial_\varphi (\Delta p v \cos \varphi) \right] u + \left[\frac{v}{a \cos \varphi} \partial_\varphi (u \cos \varphi) \right] \Delta p. \tag{A7}$$

704 The approximation here consists in using C-grid (advective) fluxes in the partial differentials
 705 on the right-hand side. Considering this as a calculation for the advective fluxes of zonal
 706 momentum, which is its physical meaning, this appears to be a valid interpretation for v . For
 707 the values of Δp and u outside the operators, we adopt the substitutions

$$\begin{aligned}
 u &=: u_o + \delta_h u + \delta'' u \\
 \Delta p &=: \Delta p_n - \delta_h \Delta p + \delta'' \Delta p,
 \end{aligned}$$

708 where

$$\delta_h \Delta p := \frac{\Delta p_n - \Delta p_o}{2}, \quad \delta_h u := \frac{u_n - u_o}{2}, \tag{A8}$$

709 and $\delta''u$ and $\delta''\Delta p$ are formally $o(\delta t)$. The increments are still understood as advective only, i.e.
 710 they exclude pressure force terms. By further using the identities

$$-\frac{\delta t}{a \cos \varphi} \partial_\varphi (\Delta p v \cos \varphi) = \Delta p_n - \Delta p_o + \frac{\delta t}{a \cos \varphi} \partial_\lambda (\Delta p u) \quad (\text{A9})$$

$$-\left[\frac{1}{a \cos \varphi} \partial_\varphi (u_o \cos \varphi) \right] v \delta t = \left(\zeta_o - \frac{1}{a \cos \varphi} \partial_\lambda v_o \right) v \delta t, \quad (\text{A10})$$

711 we finally arrive at the expression for our approximate angular-momentum conserving zonal-
 712 mean zonal wind correction:

$$\begin{aligned} \left(\int d\lambda \Delta p_n \right) \overline{\delta u} &= \int d\lambda (\Delta p_n - \delta_h \Delta p) \left[\frac{1}{a \cos \varphi} \partial_\lambda K - \zeta_{\lambda o} v \right] \delta t \\ &+ \int d\lambda \left[\frac{1}{a \cos \varphi} \partial_\lambda (\Delta p u) \delta t \right] (u_o + \delta_h u) \\ &+ \int d\lambda \left[2\delta_h \Delta p + \frac{1}{a \cos \varphi} \partial_\lambda (\Delta p u) \delta t \right] \delta''u \\ &+ \int d\lambda \delta''\Delta p [\xi_o v - \zeta_{\lambda o} v] \delta t, \end{aligned} \quad (\text{A11})$$

713 where we have used the shorthand $\zeta_{\lambda o} := \frac{1}{a \cos \varphi} \partial_\lambda v_o$.

714 We note that setting the higher-order terms to zero implies that the correction has no effect
 715 on a zonally symmetric flow. If, in addition, the flow is in an exact steady-state, then the
 716 correction always vanishes identically, regardless of these terms. It can further be shown that,
 717 if the term in K is the true gradient of the kinetic energy in the original scheme, for any values
 718 of $\delta''u$ and $\delta''\Delta p$ that are first order in δt or higher, the correction (A11) is formally third-order
 719 in δt or higher. In other words, the correction will not affect solutions that are already locally
 720 angular-momentum conserving.

721 In Equation (A11), all mass terms must be averaged over φ ; by contrast, all advective terms
 722 (in square brackets) represent fluxes as discretised according to the standard LR97 algorithm.
 723 The discretised expression of Equation (A11) thus corresponds with Equation (7). The only
 724 additional PPM calculation required to calculate this correction is the meridional advection of
 725 the partial relative vorticity, ζ_λ , with a minimal additional computational cost that is hardly
 726 detectable in CAM simulations.

C Formulation and implementation of the AM fixer in CAM-FV

As we explain in section 2.4, the fixer is based on diagnosing the global change of atmospheric AM due to advective increments only, which should vanish identically according to the continuous equations. When applied, the fixer counteracts that change at every advective sub-step; irrespectively, its time-mean increments can always be used to diagnose AM non-conservation in the simulations, in a manner that is completely independent of the physics parametrisations or boundary conditions used, and hence independent of the particular configuration of the simulations itself. All the calculations related to the fixer and the quantification of the numerical (advective) AM source are internal to the dynamical core only, indeed of its shallow-water part.

So, for each time-step and at each level k , we require the advective shallow-water equation increments to satisfy:

$$\delta \left\{ \sum_{i,j} [u_{i,j} \cos e_j + u_{i,j+1} \cos e_{j+1} + a\Omega (\cos^2 e_j + \cos^2 e_{j+1})] \cos c_j \Delta p_{i,j} \right\}_k = 0, \quad (\text{A12})$$

where the indices (i, j) refer to longitude and latitude, respectively; e_j are the latitudes of the u-velocity points of the D-grid; and c_j the latitudes of the scalar points (A-grid). The other symbols have the same meaning as in the previous section, and δ represent the purely advective increment obtained in the dynamical core, which may include the correction discussed above. The action of the fixer in this context is represented by an additional increment $\delta\varpi_k$, so that the total increment of the zonal wind becomes $\delta u_{i,j,k} + a\delta\varpi_k \cos e_j$. We obtain:

$$\delta\varpi_k = -\frac{T_k}{I_k} \quad (\text{A13})$$

where the numerical torque is

$$T_k = a \sum_{i,j} \cos e_j (\cos c_j + \cos c_{j-1}) \{ \delta u_{i,j} \overline{\Delta p_{i,j}^\varphi}(t + \Delta t) + [u_{i,j}(t) + a\Omega \cos e_j] \delta \overline{\Delta p_{i,j}^\varphi} \}_k \quad (\text{A14})$$

and the moment of inertia is

$$I_k = a^2 \sum_{i,j} \cos^2 e_j (\cos c_j + \cos c_{j-1}) \overline{\Delta p_{i,j,k}^\varphi}(t + \Delta t). \quad (\text{A15})$$

In these expressions,

$$\overline{\Delta p_{i,j,k}^\varphi} := \frac{\Delta p_{i,j,k} \cos c_j + \Delta p_{i,j-1,k} \cos c_{j-1}}{\cos c_j + \cos c_{j-1}}. \quad (\text{A16})$$

748 Equation (A13) gives the required angular acceleration of the entire atmospheric shell at model
 749 level k . The action of the “level” fixer is therefore to add an increment to the zonal wind:

$$\delta^f u_{i,j,k} = a \delta \varpi_k \cos e_j. \quad (\text{A17})$$

750 In some regions of the model domain, it is not desirable to apply a fixer, since dissipation is
 751 explicitly built into in the dynamical core formulation. This is the case near the upper boundary
 752 of CAM’s domain (the lower boundary in pressure space), where the fixer is accordingly switched
 753 off. In general, a weight $w_k \leq 1$ can be applied at each level, so that Eq.(A13) becomes

$$\delta \varpi_k = -w_k \frac{T_k}{I_k}, \quad (\text{A18})$$

754 where only a fraction w_k of the numerical torque at level k is compensated by the fixer at that
 755 level.

756 The “global” fixer applies the same solid-body rotation increment to all levels within the
 757 domain where it is required. When all weights are unity, this is simply

$$\delta \varpi_g = -\frac{\sum_i T_i}{\sum_j I_j}; \quad (\text{A19})$$

758 when $\exists k : w_k < 1$, the vertical integrals must be weighted accordingly, and the weights applied
 759 to the correction at each level, so that

$$\delta \varpi_{g,k} = -w_k \frac{\sum_i w_i T_i}{\sum_j w_j I_j}. \quad (\text{A20})$$

760 It can be seen that $\sum_k I_k \delta \varpi_{g,k} = -\sum_k w_k T_k$ so that the numerical torque associated with the
 761 domain of interest is fully compensated also by this fixer. Experimentation has shown that
 762 tapering the global fixer so as to exclude its action from levels in the stratosphere was necessary,
 763 in order to avoid distortions of the dynamics in layers where it is sensitive to small amounts
 764 of zonal acceleration; and where, moreover, thanks to the predominance of solenoidal dynamics
 765 (before gravity-wave drag, which is applied in the physics parametrisations), the dynamical core
 766 performs well in terms of AM conservation. For the latter reason, no tapering (i.e. any weights
 767 other than 1 in the valid domain, and 0 in the filtered layers near the model lid) is in fact
 768 required for the level fixer.

769 For diagnostic purposes, fixer increments are always calculated as in Eq.(A13) and provided
 770 in output. Use of the increments in Eq.(A13) lead to conservation of total AM in idealised
 771 spin-up or spin-down experiments with no physical sources or sinks of momentum (cf. Figure

772 3), as well as an accurate balance of the surface torques in Held-Suarez or Aquaplanet simu-
773 lations where only surface stresses are present (and accurately diagnosed). Hence, we obtain
774 two important conclusions. First, all numerical sources of AM indeed reside in the advective
775 wind increments of the shallow-water part of the dynamical core; second, the fixer diagnostics
776 return an accurate estimate of the apparent numerical AM source for any CAM-FV integration,
777 irrespective of physics parametrisations or boundary fluxes (including orographic form drag).